UNIVERSITY OF OKLAHOMA

GRADUATE COLLEGE

# A PALEOCLIMATE AND PALEOFIRE HISTORY FROM THE EARLY PLEISTOCENE OF UNAWEEP CANYON, NORTHWESTERN COLORADO

A THESIS

SUBMITTED TO THE GRADUATE FACULTY

In partial fulfillment of the requirements for the

Degree of

Master of Science

By

KAREN S. VALLES

Norman, Oklahoma

2024

Downloaded from SHAREOK. Persistent Handle URL: https://hdl.handle.net/11244/340313

A PALEOCLIMATE AND PALEOFIRE HISTORY FROM THE EARLY PLEISTOCENE OF UNAWEEP CANYON, NORTHWESTERN COLORADO

A THESIS APPROVED FOR THE

SCHOOL OF GEOSCIENCES

BY THE COMMITTEE CONSISTING OF

Dr. Gerilyn Soreghan, Chair

Dr. Shannon Dulin

Dr. Caitlin Hodges

Dr. Gonzalo Jiménez-Moreno

Dr. Xiaolei Lui

Copyright to KAREN VALLES 2024 ©

All Rights Reserved.

**ACKNOWLEDGEMENTS**

Foremost, I would like to express my deepest gratitude to my advisor, Dr. Lynn Soreghan, for trusting me with this project and for her continuous support, patience, and knowledge. I would also like to thank everyone on my committee: Dr. Shannon Dulin, Dr. Caitlin Hodges, Dr. Gonzalo Jimenez-Moreno, and Dr. Xiaolei Liu for their knowledge, experience, and immense support. I would also like to thank the National Science Foundation (Award Number: 1849623) for providing funding for this project. Thank you to Anders Noren, Brady Shannon, and everyone at the Core Scientific Drilling Facility (CSDF) at the University of Minnesota for welcoming us and aiding us with the core sampling. Thank you to Mackenzie Flynn for enduring and assisting me in sampling and to Ryne Andrews, Parker Lynn, Nick Evett, and Ruby Pearsons for assisting me with the sample preparations and analysis. Lastly, thank you to my parents, Gildardo and Claudia Valles, and my siblings, Stephanie and Zenith, for supporting me throughout this process.

Table of Contents

List of Figures ..... vii
Abstract ..... viii
1. Introduction ..... 1
2. Geologic and Paleoclimatic Setting ..... 4
3. Depositional Setting ..... 8
4. Palynomorphs Analysis ..... 10
    4.1 Basal Phase ..... 11
    4.2 Lower Cold Phase ..... 11
    4.3 Lower Warm Phase ..... 11
    4.4 Upper Cold Phase ..... 12
    4.5 Upper Cold Phase ..... 12
5. Methods ..... 12
    5.1 Core Sampling ..... 12
    5.2 Additional Palynomorph Sampling ..... 13
    5.3 Charcoal Particle Processing ..... 13
    5.4 Carbon-Nitrogen-Sulfur Analysis ..... 14
    5.5 Glycerol Dialkyl Glycerol Tetraether (GDGT) Analysis ..... 14
6. Results ..... 17
    6.1 Age Control and Estimated Sedimentation Rates ..... 17
        6.1.1. Age Control ..... 17
        6.1.2 Sedimentation Rates ..... 17
7. Charcoal Accumulation Rates ..... 18
8. Charcoal Concentrations ..... 19
    8.1 Total Charcoal ..... 19
    8.2 Macro-Charcoal ..... 19
9. Branched GDGTs ..... 20
10. Magnetic Susceptibility ..... 20

10.1 Basal Phase ..... 20
10.2 Lower Warm Phase ..... 20
10.3 Upper Cold Phase ..... 21
10.4 Upper Warm Phase ..... 21
10.5 X-ray Fluorescence (Zr counts, Ti/Al and Mg/Al count ratios) ..... 21
11. Discussion ..... 22
11.1 Basal Phase ..... 22
11.2 Lower Cold Phase – Glacial ..... 23
11.3 Lower Warm Phase – Interglacial ..... 24
11.4 Upper Cold Phase – Glacial ..... 25
11.5 Upper Warm Phase – Interglacial ..... 26
11.6 Comparison of Other Studies ..... 27
12. Conclusions ..... 28
References ..... 30
Tables & Figures ..... 51

List of Tables & Figures

Table 1: Well Locations and Depths ..... 51
Figure 1: Unaweep Canyon Coring location ..... 52
Figure 2: Glaciation near Unaweep Canyon ..... 53
Figure 3: Massey #1 and UDR 1A Depths ..... 54
Figure 4: Condensed UDR 1A Core ..... 55
Figure 5: Pollen Assemblages ..... 56
Figure 6: Total and MacroCharcoal Accumulation Rate (CHAR) ..... 57
Figure 7: Magnetic Susceptibility (MS) ..... 58
Figure 8: Comprehensive paleoclimate and paleofire indicators for UDR 1A ..... 59

**ABSTRACT**

Lacustrine systems capture high-resolution records of continental climate, including information on paleotemperatures, hydroclimate, and paleofire activity. An increasing number of studies have reported paleoclimate and paleofire records from Holocene and upper Pleistocene sedimentary archives across various regions of the arid western U.S., shedding light on possible future scenarios of linked climate-fire regimes attendant with continued climate change; however, records from older intervals are rare to nonexistent. Here, we report on an investigation of paleoclimate and paleofire from an upland lake of the early Pleistocene that records accumulation prior to the Mid-Pleistocene Transition. We recovered an exceptionally long (147 m) core from an early Pleistocene (~1.4-1.3 Ma) lake buried ~200 m subsurface in Unaweep Canyon, a high-relief, upland system of the Uncompahgre Plateau in western Colorado that hosts a thick sediment fill. The age (~1.4-1.3 Ma) is based on cosmogenic-nuclide dating of a previous, correlative section. The sediment comprises predominantly mass flow event beds such as turbidites, with grain sizes ranging from sand to mud. Over the ~147 m of the lacustrine section, prominent color variations occur: two intervals (20 - 32 m thick) exhibiting mostly red and ochre (oxidized) colors alternating with two intervals (35 - 53 m thick) exhibiting mostly drab olive to dark gray (reduced) colors. These color variations correspond to changes in palynological assemblages that indicate two cold-warm variations—inferred glacial-interglacial cycles—with glacials represented by high values of *Picea* and *Abies* pollen and generally oxidized colors, and interglacials represented by high values of *Artemisia* and *Pinus* pollen and generally drab colors. Climatic conditions are further explored through the variance of magnetic susceptibility (MS), Zr, Ti/Al and Mg/Al ratios between the cycles: glacials exhibit higher averages of MS, Zr, Ti/Al and Mg/Al, suggesting increased detrital input and runoff, interpreted to record wetter

conditions. Charcoal accumulation rates vary between the glacial-interglacial hemicycles, with higher concentrations in warmer (interglacial) conditions. Additionally, mean daily insolation patterns were calculated for the general Unaweep region, demonstrating that higher charcoal accumulation rates correspond with times of higher insolation. Overall, the UDR 1A core records that interglacials at the beginning of the mid-Pleistocene transition record warmer and drier conditions that were accompanied by increased frequency of fire occurrence and intensity.

## INTRODUCTION

Lake sediment records archive biological, physical, and chemical indicators of climate in the form of sediment attributes, pollen, charcoal, and molecular fossils, (Fritz 1996; Zolitschka & Enters, 2009) thus contributing to our knowledge of continental paleoclimate, especially for the Quaternary (Kaufman et al. 2020; Zimmerman & Wahl, 2020). In the western U.S., and specifically the Rocky Mountain region, preservation is biased on locations where erosion is minimal, meaning that the majority of these records cover the mid-late Pleistocene and Holocene, with few if any records extending to the early Pleistocene (Davis, 1998; Allstädt et al., 2021; Staley et al. 2022).

During the late Pliocene to early Pleistocene, global climate progressively cooled, ultimately resulting in glaciation in the Northern Hemisphere (Maslin et al., 1998; Raymo et al., 2006; Sosdian & Rosenthal, 2009). A distinguishing, but poorly understood, feature of the Pleistocene was the intensification of northern hemisphere glaciation (Ruggieri et al., 2009), accompanied by expansion of continental ice sheets, and a shift in the behavior of the glacial-interglacial cycles across an interval known as the Mid-Pleistocene Transition (MPT) (~1.25 – 0.7 Ma; Herbert 2023). Whereas glacial cycles during the early Pleistocene behaved in an unstable manner, characterized by relatively low amplitudes and short (obliquity) frequency, glacial cycles after the MPT record higher amplitudes and longer (eccentricity) periodicity (Herbert 2023; Yan et al., 2023). This transition likely reflects a confluence of many factors (Herbert 2023), including decreased levels of atmospheric carbon dioxide ($CO_2$), driving temperatures lower (Willeit et al., 2019; Legrain et al., 2023) relative to early Pleistocene levels, which ranged as low as pre-industrial levels (280 ppm) and even higher than near-term anthropogenic levels (500 ppm) (Wang et al., 2018; Da et al., 2019; De la Vega et al., 2020).

Although a growing number of studies are addressing the MPT (Chalk et al., 2017; Sun et al., 2019; Bajo et al., 2020; Berends et al., 2021; Yamamoto et al., 2022) and many more cover the late Pleistocene and Holocene in the western United States (U.S.), few studies have targeted the early Pleistocene (pre-MPT) in the western U.S. (Davis, 1998; Allstädt et al., 2021; Staley et al. 2022).

Given that the early Pleistocene had an atmospheric composition similar to the modern, research on this interval can contribute to our understanding of the effects of anthropogenic climate change (Berends et al. 2021). One of the many effects of anthropogenic climate change is the relationship between climate warming and global wildfire activity (Marlon, 2020). Marlon et al. (2008) found that overall, global burning declined after 1870 owing to large-scale expansion of intensive grazing, agriculture, commercial development, and active fire management, but that rural areas with less land management (e.g., western U.S.) experienced an increase in fire risk, intensity, and frequency owing to human activity and ongoing climate change.

Several studies have suggested that increased wildfire frequency will accompany the continued warming associated with modern climate change, owing to the positive feedbacks of rising temperatures, earlier snowmelt, and increased droughts, all exacerbated further by wildfires (Jolly, 2015; Schoennagel, 2017). In turn, wildfires affect other aspects of the Earth system such as vegetation cover and erosion (Pierce et al. 2004; Cannon et al. 2008). Liu et al. (2013) posited that fire potential will increase in several areas of the US, including the Southwest and Southeast, the northern Great Plains, the Pacific coast, and the Rocky Mountains. In the Rocky Mountains specifically, Riley and Loehman (2016) projected a 48% increase in fire potential for the future (2030-2059), attributable to longer periods of favorable fire weather: hot temperatures, dry weather, and low moisture.

One way to better understand future climate-fire dynamics is to reconstruct paleofire histories using indicators such as dendrochronology, tree fire scars, and charcoal—the latter a popular direct indicator since the mere presence of charcoal marks the occurrence of a fire event (Whitlock & Larsen, 2002). Charcoal particles can be transported via rainwater runoff, rivers, and wind (Iglesias et al., 2015) and accumulate in various environments including wetlands and peat bogs, ocean floors, rivers, and lakes. Charcoal analysis on sediment cores from lacustrine environments is thus highly desirable owing to the ability of lakes to record an exclusive, closed-system environment (Marlon, 2020).

The characteristics of fire events spanning centuries are studied to create fire regimes under the influence of different fire variables including fuel type, seasonality, intensity, frequency, spatial distribution, and attributes of the surrounding ecosystem (Jurvelius, 2004; Bowman et al. 2009). Climate and vegetation greatly affect fire activity, including severity, frequency, duration, and therefore charcoal production (Marlon, 2020); e.g. burning biomass generally decreases during glacial intervals, and—conversely—increases during interglacial intervals due to an increase of insolation causing warmer and drier climate conditions (Power et al. 2008; Daniau et al. 2010). Owing to this relationship, previous studies have utilized charcoal concentration variability as a paleoclimate proxy (Daniau et al., 2007; Huang et al., 2020; Zhao et al., 2023).

The increase in wildfire frequency and intensity in the western US, attendant with the effects of a warming climate, have ignited increased interest in integrated paleoclimate-paleofire studies to shed light on current and future climate-fire dynamics (Westerling et al., 2006; Higuera et al., 2007), and studies focusing on the Colorado Plateau region demonstrate this (Bigio et al. 2010; Jenkins et al. 2011; Briles et al., 2012; Roos & Swetnam, 2012; Mogen, 2018). However,

to date, studies from this region focus almost exclusively on the Holocene. The lack of accessibility and preservation of sediment records older than the Holocene in the western U.S. is apparent in paleofire reviews and databases that focus primarily on Holocene records (Marlon et al., 2013; Sanchez Goñi et al., 2017), and pre-Quaternary paleofire studies are even fewer (Jasper et al., 2021). Like other paleoclimate proxies, paleofire indicators, especially those from lacustrine archives, are commonly limited by preservation and nondeposition (Mishra, 2023).

In this study, I focus on an early Pleistocene paleolake preserved in the subsurface of Unaweep Canyon of the Uncompahgre Plateau, in the northeastern-most Colorado Plateau. A serendipitous confluence of events-- the landslide blockage of a high-relief landscape occupied by a large river-- created a relatively large lake that persisted for a significant interval (Kaplan, 2006). This system captures a unique record spanning several glacial-interglacial cycles of the early Pleistocene, thus providing a window on paleoclimatic variations and associated shifts in paleofire regimes, landscape erosion, and lacustrine sedimentation within an upland setting of the Rocky Mountains.

## GEOLOGIC AND CLIMATOLOGICAL SETTING

Unaweep Canyon (38.790556°N, 108.655°W, 2148 m above sea level [a.s.l]) is located in Western Colorado, bisecting the Uncompahgre Plateau on the northeastern Colorado Plateau (Fig. 1; Soreghan et al., 2015). The canyon's formation is controversial: Aslan et al. (2008) attributed the canyon entirely to late Cenozoic fluvial erosion, whereas Soreghan et al. (2007, 2008, 2014, 2015) hypothesized a late Paleozoic glacial origin and Permian burial followed by Cenozoic fluvial exhumation and abandonment by the ancestral Gunnison River. Soreghan et al. (2015) also documented a Pleistocene lacustrine interval preserved within the subsurface of

Unaweep Canyon, buried beneath ~150 m of Pleistocene fanglomerate deposits; cosmogenic dating indicates that the ancestral Gunnison River abandoned its course through Unaweep Canyon ca. 1.41± 0.19 Ma, and lacustrine infilling ceased by ca. 1.34 ± 0.13 Ma (Balco et al., 2013). This lacustrine interval is thought to reflect in part a mass-wasting event that blocked the ancestral Gunnison River prior to the abandonment of the canyon by the river (Soreghan et al., 2015).

Given the lack of exposure of the deposits termed paleo-lake Unaweep, the size of the lake and its catchment area can only be approximated using the modern landscape configuration, assuming that the lake filled to the level of the upper-most preserved sediments recovered from a previous coring campaign (Marra, 2008; Soreghan et al., 2015). The modern-day catchment of the canyon, ranging from the western mouth of the canyon to slightly east of Unaweep Divide, is estimated to be ~487 $km^2$, excluding the area of paleo-lake Unaweep, estimated to be ~30 $km^2$. The relatively steep walls of Unaweep Canyon consist of Proterozoic igneous and metamorphic basement rimmed by Mesozoic sedimentary rocks, exhibiting a modern-day relief of up to ~700 m in the inner (Precambrian) gorge. However, owing to the thick sedimentary fill in Unaweep Canyon (>350 m), and considering maximum elevation of the canyon rims, the estimated maximum paleo-relief during the initial formation of the lacustrine system ranges up to ~1000 m (projecting towards the south and north rims, respectively) (Table 1, Fig. 1).

Climate in the southwestern U.S. region is influenced by the North American monsoon (NAM), a shift in the westerly winds towards the north that provides increased precipitation during the summer (June-July-August) months (Douglas et al. 1993; Adams & Comrie 1997). During glacial intervals of the late Pleistocene, extensive glacial coverage and cooler climate weakened the NAM (Bhattacharya et al., 2018), causing drier conditions in the immediate area

of western Colorado, but generally wetter conditions across the western U.S. (Oster et al., 2015). No modern climatological data exists for the area—including the study site within Unaweep Canyon; however, historical climate records are available for Gateway, Colorado, located approximately 15 km west from the UDR 1A drilling site, at an elevation (1,416 m asl) ~500 m lower than that (1924 m asl) of the study site (Fig. 1). The Gateway records report a maximum mean annual temperature (MAT) of 20.2 °C and a minimum MAT of 4.1 °C, from 1947 through 2016 (Western Regional Climate Center). Today, the mean annual precipitation (MAP) is 28.8 cm, with the lowest precipitation during June and the highest during July-August-September-October (Western Regional Climate Center, 2024).

Cole & Young (1983) suggested Pleistocene glaciation of Unaweep Canyon owing primarily to its distinctive geomorphology—namely, apparent U-shaped cross section and features that resemble truncated spurs and hanging valleys along its margin. However, this hypothesis failed to gain traction owing to the lack of convincing glacial deposits, and—in particular—the lack of evidence for Pleistocene glaciation atop the Uncompahgre Plateau, as the elevations lie predominantly below terminal moraine elevations of recent/Last Glacial Maximum (LGM) glaciations in the greater region (Fig. 2; Leonard, 1989). However, several studies have documented Pleistocene glacial activity in the form of till and outwash in (generally) higher-elevation regions of surrounding mountains and plateaus, such as atop Grand Mesa (~3050 m asl) (Yeend, 1969; Cole and Sexton, 1981) approximately 50 km northeast of Unaweep Canyon. Yeend (1969) posited that Grand Mesa hosted an ice cap that flowed down major, north-facing stream valleys with elevations ranging from ~3050 m to as low as ~1646-1768 m during recent glaciations; Yeend (1969) attributed the unusually low elevations of ice tongues on the north slopes of Grand Mesa to its extensive, high-elevation catchment area that promoted development

of an ice sheet, and the existence of deep valleys on the north flank of the mesa. However, Sinnock (1978) and Cole and Sexton (1981) disputed the till interpretation, favoring mass-flow for the deposits. Other studies have documented LGM-early Holocene glacial activity in areas such as the Aquarius Plateau, Utah, and San Francisco Peaks, Arizona (Richmond 1986; Marchetti et al., 2017).

Evidence of glaciation during the early to late Pleistocene locally on or near the Colorado Plateau has also been reported. The San Juan Mountains (~4360 m asl), approximately 135 km southeast of Unaweep Canyon, preserve recent (2.6 – 2.2 Ma to >17.1 ka) glacial moraines and terraces along the Animas River, with the lowest-elevation moraine at 2987 m (Atwood & Mather, 1912; Leonard 1984; Gilliam 1998; Johnson et al., 2017). The La Sal Mountains (~3788 m asl), ~50 km southwest of Unaweep Canyon, exhibit evidence of six Pleistocene glaciations at varying elevations from ~3535 m, in the Gold Basin Formation, to as low as ~2072 m in the Harpole Mesa Formation (Richmond, 1962; Richmond & Fullerton, 1986). However, the lowest elevation of terminal moraines documented in La Sal Mountains is an outlier as all average elevations of terminal moraines of other formations are above 2500 m. Both the average elevation of the Uncompahgre Plateau (~2895 m) and the highest point within Unaweep Canyon (Unaweep Divide, at ~2148 m) are generally lower than the lowest-elevation evidence for Pleistocene glaciation in the greater region (excepting Grand Mesa); this, together with the lack of Pleistocene glacial deposits (Lohman, 1981; Scott et al., 2001) are most consistent with the interpreted absence of Pleistocene glaciation in Unaweep Canyon.

Today, vegetation in surrounding areas and at lower elevations (1400 m asl) is dominated by salt desert shrubs, such as shadscale or saltbrush (*Atriplex spp.*) and sage brush (*Artemisia tridentata*), which thrive in arid and high-saline environments (Branson et al. 1976). At higher

elevations (1500 m asl) Pinon pina (*Pine edulis*) and Utah Juniper (*Juniperus osteosperma*) are prevalent (Young, 1983). Ponderosa pine (*Pine ponderosa*) and Douglas fir (*Pseudotsuga menziesii*) predominate in forests above ~2400 m asl (Kolb & Robberecht, 1996). At even higher elevations (3350 m asl), Engelmann spruce (*Picea engelmannii*) and subalpine fir (*Abies lasiocarpa* Nutt.) are the most dominant tree species, often withstanding high winds and low-temperature conditions (Wardle et al., 1968).

## DEPOSITIONAL SETTING

As noted above, previous (2004) drilling (Massey #1) in Unaweep Canyon found the remnants of paleolake sediment buried beneath ~150 m of alluvial material (Fig. 3). Marra (2008) documented the sediment core from drilling project Massey #1 and found an upwardly coarsening fill pattern comprising ~143 m of sandy to clayey lacustrine sediment. Three different facies are described within the lacustrine interval: 1) fine-grained olive gray clay, with local bioturbation, and yellowish-brown sandy clay; 2) massive, unconsolidated yellowish-brown medium to coarse sand, with granules and pebbles (<3.5 cm); and 3) fine to medium-grained clayey to carbonaceous sandstone near the top of the interval. The lacustrine interval was capped by an ~8 m transitional unit of paleosols, separating the lacustrine interval and the alluvial material, with the lacustrine interval inferred to represent a progradational deltaic system (Marra, 2008).

Drilling and coring of the UDR-1A borehole began in February 2022 and progressed to a total depth of ~426 mbs (meters below surface) (Table 1). Owing to the expense of coring, recovery focused on the deepest sediment preserved in the canyon; hence, guided by previous

seismic imaging (Patterson et al., 2021), the upper ~200 m of drilling was destructive, with no core recovery. Based on correlation to previous coring at sites Massey #1 (2004) and its adjacent twin Massey #2 (2006) (both ~6 km east of UDR #1; Fig. 1), this upper 200 m interval penetrated Pleistocene alluvial-fan material (Marra, 2008) and approximately 97 m of the upper part of the paleolake section (Harris, 2023). A total of ~226 m of core (sediment and basement) was recovered from UDR #1, and sedimentological analyses conducted by Harris (2023) are summarized here. Harris (2023) found that event-like sediment gravity flows predominated throughout the cored interval, with generally coarser sand- and pebble-sized sediments near the basal section (~20 m) of the lacustrine interval, and finer sediments-- fine clay to medium sand thereafter. The core exhibits strikingly contrasting colors in different intervals—ranging generally from drab, olive-grays (reduced) in two intervals ranging from 35 to 53 m thick, alternating with two intervals of ochre or deep reddish-brown (oxidized) colors ranging from 32 to 20 m thick. All features assisted in further delimiting six facies and sub-facies (Harris, 2023; Fig. 4). Both olive-gray and ochre intervals are dominated by upwardly fining sequences (mass-flow beds). Differences in sedimentology between the two color intervals are minimal, however sediments in the olive-gray intervals are generally finer grained, dominated by very fine sand or fine to coarse sand (medium sorted and sub-angular shaped) at the sequence bases and clay at tops, with individual beds ranging from ~1-50 cm respectively. These intervals commonly exhibit bioturbation at the bed tops, suggesting oxic conditions, and convoluted beds within the sequences. Also present, albeit less commonly, are beds of massive sand/gravel capped by clay/silt with no gradation in between, and massive, unconsolidated silt and clay matrix with embedded basement clasts (~1 cm). Ochre colored intervals exhibit coarser sediments at the sequence bases, ranging from medium coarse sand to granules and pebbles that grades into clay

at the sequences tops. Sequences in the ochre color intervals  range from ~1-25 cm in thickness. have thicker bases, thinner tops, and exhibit less bioturbation, convoluted bedding, massive sand/gravel capped by clay/silt, and embedded basement clasts.

**Palynomorph Analysis**

Dr. Gonzalo Jiménez-Moreno conducted palynological analyses to calculate pollen ratios and percentages. Previous paleoclimate studies have used pollen ratios to outline paleo-environment and climate change (Anderson et al., 2020) and many others have used palynomorph assemblages for early Pleistocene, and older, sites (Adam et al., Groot, 1991; Davis, 1998; Allstädt et al., 2021).

*Artemisia*/*picea* ratios, *Pinus*/*Picea+Abies* ratios, and desert shrubs percentages, were used to identify two different climatic states within the cored lacustrine section (Fig. 5). *Artemisia*/*Picea* ratios have been used as indicators of warming or cooling climate transitions, higher ratios indicate a decrease in average temperature (Jiménez-Moreno et al. 2008, 2011, 2023; Johnson et al. 2013) using the following equation (1):

$$\frac{Artemisia}{Picea} ratio = \frac{Artemisia - Picea}{Artemisia + Picea} \quad (1)$$

A *Pinus*/*Picea+Abies* ratio was also utilized, higher ratios indicating warming climatic conditions (Beaudoin, 1986; Kim et al., 2023). Lastly desert shrub percentages were used as indicators for warm climate conditions, higher ratios indicating warm and dry climate conditions (Peaple et al., 2022) since they thrive in areas that receive precipitation prior to the growing season (Dilts et al. 2015).

Based on these ratios and percentages, four distinct pollen zones were identified and are described below (Fig. 5):

*Basal Phase (~332-339 mbs)*

The basal 7 m comprises a reddish-brown, coarse sand interval and only one sample through this interval yielded pollen. The desert shrub percentage (25%) and *Pinus*/*Picea*+*Abies* ratio (0.1) resembles the core's other cold climate phases. However, the *Artemisia*/*Picea* ratio for this phase is 0.8, ~0.23 higher than the average of the other cold climate phases.

*Lower Cold Phase (~308 – 332 mbs)*

The lower cool phase provided 3 samples with sufficient pollen assemblages needed for interpretation. This phase is characterized by relatively low *Artemisia*/*Picea* ratios (average ~ .44, standard deviation (SD) = 0.12) and desert shrubs percentages (~19.5, SD = 3.8), indicating cold and relative pluvial conditions. Three of the four samples collected in this phase contained a low *Pinus*/*Picea*+*Abies* ratio (~0.4, SD = 0.09), with one sample exhibiting a ratio of ~0.6.

*Lower Warm Phase (~255 – 308 mbs)*

The lower warm phase yielded 28 samples with sufficient pollen assemblages needed for interpretation. *Artemisia*/*Picea* ratios are relatively consistent throughout this phase (~.86 average ratio, SD = 0.16), dropping below 0.6 in only three depths. *Pinus*/*Picea*+*Abies* ratios vary, however, still maintain a high overall average (~.77 average ratio, SD = 0.18). Although desert shrub percentages remain relatively low (~30% average, SD = 11.75), there is a notable increase from the previous wet hydroclimate, indicating warmer and drier climate conditions relative to the previous phase.

*Upper Cold Phase (~235 – 255 mbs)*

The upper cold phase yielded 6 samples with sufficient pollen assemblages needed for interpretation. This phase exhibits a shift into lower values of *Artemisia*/*Picea* (~ .49 average ratio, SD = 0.25) and *Pinus*/*Picea*+*Abies* (~0.458, SD = 0.25) ratios and desert shrub percentages (~19.8, SD =4.73). These values are interpreted to record relatively cold and humid climate conditions. However, there is one sample, at ~247.5-248 mbs, where all three pollen assemblages increase, coinciding with a change in sediment color and an increase in raw charcoal particles, possibly indicating a short interval of warmer and drier climate conditions.

*Upper Warm Phase (~200 – 235 mbs)*

The upper warm phase provided 22 samples with sufficient pollen assemblages needed for interpretation. An increase in all pollen assemblages occurs during this phase: *Artemisia*/*Picea* ratios remain consistent throughout this phase, uniformly above 0.6 (~0.91 average ratio, SD = 0.08) and the *Pinus*/*Picea*+*Abies* ratio remains above 0.3 (~0.7 average ratio, SD = 0.15). The desert shrub percentages (62-19%) are the highest in amount and variation of any interval throughout the core, and the highest average (~32% average ratio, SD = 10.9). These pollen assemblages indicate a shift into warm and dry climate conditions.

## METHODS

*Core Sampling*

The total ~226 m of core (sediment and basement) was collected using an HQ3 impregnated diamond bit with wireline core recovery. The core was recovered in polyurethane

liners, which were capped, labeled, and shipped to the University of Minnesota Continental Scientific Drilling (CSD) facility, and refrigerated. Prior to splitting, the core was scanned using a Geotek Standard Multisensory Core Logger (MSCL) to measure magnetic susceptibility (MS), gamma density, P-wave velocity and amplitude, natural gamma radiation, and electrical resistivity in 0.5 cm increments. X-ray fluorescence (XRF) geochemistry was also collected at 0.5 cm increments for thirty different element count fluctuations.

Once the cores were split and photographed, lithologic description and sampling for sedimentology was done, including sand petrography, smear slides, provenance and magnetic mineralogy (reported in Harris, 2023 and summarized in the Results section, p. 15), in addition to preliminary palynological analyses. Briefly, sampling was done (by Harris, 2023) for smear slides (n = 49), thin sections (n = 23), and sand petrography (n = 34). Additionally, samples (n = 35) for preliminary palynological analyses were taken at an average interval of 3 m, processed by Global Geolabs, and analyzed by G. Jiménez-Moreno in order to guide further sampling. In summer 2023, additional sampling was conducted to enhance the palynological dataset, and to sample for charcoal, carbon-nitrogen-sulfur, and organic geochemical analyses, as detailed below.

*Palynomorph Sampling*

Additional palynomorph samples (n =59, ~1 $cm^3$) were taken at vertical intervals of approximately 2.5 m throughout the UDR-1A core. The samples were processed by Global Geolabs, utilizing the same processing method as listed above, and analyzed by G. Jiménez-Moreno.

*Charcoal Particle Processing*

For charcoal analyses, samples (n = 1500) were collected from the UDR-1A core at vertical intervals of ~10 cm, with care taken to avoid intervals affected by drilling disruptions or drilling mud invasions. Given the common occurrence of mass flow units, samples at ~10 cm were taken at random i.e., without any regard or bias to intervals enriched in charcoal. Due to time constraints for this thesis, analysis occurred on a coarser resolution of ~50 cm, for a total of 267 charcoal analyses. Charcoal concentrations (particles/gram) of the UDR-1A core were stratigraphically quantified using charcoal particle counting. Samples (n = 267) were first weighed and then soaked in a .008 M (5g/L) solution of sodium hexametaphosphate, then wet sieved using 250 μm and 125 μm sieves with DI water. Each sample and fraction were transferred to a gridded petri dish and charcoal particles were identified and counted using magnification under bright-field conditions.

*Carbon-Nitrogen-Sulfur (CNS) Analysis*

Splits of the samples collected for charcoal analysis were processed for carbon-nitrogen-sulfur (CNS) analysis. For each of the 267 samples, approximately 0.5 g was dried (50 $^{o}$C) then ground to a powder and transferred to glass vials. Approximately 0.02 g of sample were used for both rounds of CNS analysis. During the first round, samples were analyzed for total carbon (TC), nitrogen, and sulfur concentrations using the organic elemental analyzer vario El cube. Each sample was then treated with ultra-pure water, various hydrochloric acid (HCl) solution concentrations (0.1 N, 1 N, and 6 N) to dissolve any carbonate, and then dried. After HCl treatment, the samples were reweighed and analyzed for total organic carbon, nitrogen, and sulfur concentrations using the Vario El cube.

*Glycerol Dialkyl Glycerol Tetraether (GDGT)*

Given the thickness of core, a subset of 32 samples were selected for GDGT analysis, with selection based on the palynology results (Fig. 5) that indicate both "warm" (hypothesized interglacial) and "cold" (hypothesized glacial) climate states. Due to the feasibility of sampling and processing, 16 samples were selected in each of two intervals that capture each climate end-member state. The uppermost cored interval begins at ~200 mbs, is ~45 m thick, and captures a "warm" climate state. Throughout this section, 18 samples were selected at an average interval of 250 cm. The subjacent section of 20 m thickness begins at ~245 mbs and captures a "cold" climate state. In this section, 16 samples were selected at an average interval of 111 cm.

GDGTs are membrane lipids synthesized by archaea and some bacteria (Schouten et al. 2013). GDGTs were extracted from the samples using a two-extraction method, to produce the total lipid extract (TLE). To begin this process, samples were oven-dried at 80 ºC and powdered. Approximately .08 g to 1 g per sample was used for the extraction process. Samples were treated using 1.5 ml of a 1:1 solution of DCM:MeOH (dichloromethane:methanol), sonicated, dried, and then treated with 1.5 ml of acetone, sonicated, and dried again. After the two extraction treatments, the samples were treated with 1 ml of 1:1 DCM:MeOH solution, dried, and treated with 1 ml of MeOH. The TLEs from each sample were analyzed and identified using a high-performance liquid chromatography mass-spectrometry (HPLC-MS).

Four structurally diverse GDGT groups were found across the 32 samples analyzed including isoprenoid, branched, crenarchaeol, and OB-GDGTs. Isoprenoid GDGTs are characterized by the number of cyclopentane molecules they hold, which increase with increasing temperatures and change in their structural chemistry and mass (Schouten et al. 2013). Branched or brGDGTs are synthesized by bacteria and their structure differs in the amount of methyl groups and cyclopentyl molecules (Weijers et al., 2007b). The presence of GDGTs in the

samples was identified using the Agilent MassHunter Qualitative Analysis Software, based on the accurate masses, retention times and tandem mass spectrometry (ms/ms) pattern. Due to the absence of crenarchaeol isomer molecules in 29 of the samples, we were unable to use isoGDGTs as a paleotemperature proxy ($TEX_{86}$). Instead, brGDGTs were used as a proxy for pH of soils adjacent to lacustrine settings and mean annual temperature (MAT). Peak detection of branched GDGTs was performed at mass-to-charge (m/z) ratios 744 for the $C_{46}$ standard, 1022 (Ia), 1020 (Ib), 1018 (Ic), 1036 (IIa), 1034 (IIb), 1032 (IIc), 1050 (IIIa), 1048 (IIIb), and1046 (IIIc). GDGT compound peak areas were standardized using the following equation (2):

$$x = \frac{compound\ peak\ area}{\text{standard peak area}} * amount\ of\ sample\ inject\ into\ auto\ analyzer * (\frac{100}{sample\ weight})/1000 \quad (2)$$

pH of adjacent soils and MAT were calculated utilizing the ratios of the brGDGTs to calculate cyclization and methylation of branched tetraethers, CBT and MBT (equations 3 and 4) respectively (Weijers et al., 2007).

$$MBT = \frac{[I+Ib+Ic]}{[I+Ib+Ic]+[II+IIb+IIc]+[III+IIIb+IIIc]} \quad (3)$$

$$CBT = \frac{[Ib]+[IIb]}{[I]+[II]} \quad (4)$$

calculation method, proposed by CBT and MBT results were used to calculate the MAT using equation (5) (Wiejers et al., 2007).

$$MBT = 0.122 + 0.187 * CBT + 0.02 * MAT \quad (5)$$

## RESULTS

### Age Control and Estimated Sedimentation Rates

*Age Control*

Chronological control was based initially on cosmogenic nuclide dating of the Massey #1 core, and subsequently constrained using the palynologically defined climate cycles. Balco et al. (2013) estimated that lacustrine sedimentation began ~1.41 ± 0.19 Ma and ceased at 1.34 ± 0.13 Ma for the Massey #1 core, which recovered the entire lacustrine interval. However, as noted above, the UDR 1A borehole was destructively drilled to 200 mbs, and thus the core recovered only the lower 140 m (~60%) of the lacustrine section.

*Sedimentation Accumulation Rates (SAR)*

The cosmogenic dating results, even considering the error margins, clearly indicate that the lake existed in early Pleistocene time—prior to ~1.2 Ma at youngest, and thus pre-dates the Mid Pleistocene Transition (MPT). Furthermore, the palynological results indicate that the UDR 1 core penetrates two cool-warm climate phases (assuming the basal-most 7 m is a transitional interval), which we here interpret as glacial-interglacial cycles. Given that such cycles followed an obliquity periodicity prior to the MPT, we infer that the two complete cool-warm cycles recorded in our dataset represent obliquity-scale cycles, each of ~41 ky duration.

Following this reasoning, we then calculate average sedimentation rates based on cycle thicknesses and assuming a 41 ky duration for each cycle (ie, cool-warm couplet). Given a thickness of the lower cycle (cool-warm couplet) of ~95 m implies ~0.23 cm/yr for this cycle; the upper cycle spans ~55 m, implying an average sedimentation rate of ~0.13 cm/yr.

Various factors affect sedimentation rate, including amount of sediment available for deposition, basin size, bedrock geology, climate, and--most importantly-- runoff and relief (Syvitski, 2013). Sedimentary basins with high relief (estimated to have been 1100 m asl. in Unaweep during the formation and duration of the paleolake) generally have higher rates of deposition relative to those with low relief (Milliman and Syvitski, 1992; Syvitski, 2013). Local relief in Unaweep Canyon at the time of the damming event that formed the paleolake was quite substantial-- ~1000 m, presumably promoting higher sedimentation rates overall early in the history of the lake.

**Charcoal Accumulation Rate**

Using charcoal counts for each depth, Charcoal Accumulation Rate (CHAR; particles/$cm^2$/yr) was calculated by multiplying total charcoal concentrations per depth (particles/$cm^3$) by the sediment accumulation rate (SAR in cm/yr). CHAR is calculated to minimize effects caused by sedimentation rate on charcoal concentrations (Withlock et al., 1996; Clark et al., 1998). Fire history reconstruction requires the separation of charcoal particles concentrations into two categories: “background” charcoal, deposited during non-fire events, and “peak” charcoal, deposited during a fire event (Ali et al., 2009). CharAnalysis (Higuera et al., 2009) is a popular software that analyzes charcoal data by using diagnostic and analytical components to separate the concentrations into low- and high frequencies based on concentrations (per $cm^3$) and the estimated sedimentation rate. However, for unknown reasons, the CharAnalysis software returned errors when attempting to apply it to the UDR 1A dataset. Thus, charcoal accumulation rates (CHAR) were analyzed only as a time series (Anderson et al. 2020).

**Charcoal Concentrations**

*Total Charcoal*

Charcoal particles occur in ~61% of the 264 samples analyzed. Total (>250 μm and >125 μm) raw charcoal counts, not normalized by mass, vary greatly throughout the UDR 1A core, ranging from 0 to 450 particles counted. Total charcoal influx or charcoal accumulation rate (CHAR; particles/$cm^2$/yr) varies throughout the core, the highest concentration at 20 particles/$cm^2$ (Fig. 6). Average total CHAR per samples is lowest in the lower 'cool' phase (~308-340 mbs) with an average of 0.214 particles/$cm^2$/yr. Average total CHAR increased by over an order of magnitude during the lower 'warm' phase (~255-308 mbs, 2.508 particles/$cm^2$/yr), then decreased again in the upper 'cool' phase (~235-255 mbs, 1.177 particles/$cm^2$/yr). The highest average of total CHAR occurs during the upper 'warm' phase with an average of 3.556 particles/$cm^2$/yr.

*Macro-Charcoal*

Macro-charcoal (>250 μm) raw charcoal counts vary greatly throughout the core, ranging from 0 to 271 particles counted. Macro-charcoal CHAR generally increases from the base to the top of the core (Fig. 6) The average CHAR per sample is lowest in the lower 'cool' phase with an average 0.214 particles/$cm^2$/yr. The overlying lower 'warm' phase records an increase in average CHAR per sample (0.904 particles/$cm^2$/yr), and the next interval, the upper 'cold' phase (~235-255 mbs), exhibits a similar CHAR (1.37 particles/$cm^2$/yr). The average CHAR per sample peaks in the fourth and upper 'warm' phase (~200-235 mbs) with 1.681 particles/$cm^2$/yr. Although we were not able to utilize the CharAnalysis software for determining fire events, CHAR calculations were used to determine potential fire events.

***Branched GDGTs***

Out of the 32 samples prepared for GDGT analysis, 10 samples from the upper cool phase yielded insufficient or missing branched GDGT peak area data. Unfortunately, MAT data of the sampled upper 'warm' and upper 'cold' phases provided unrealistic results and thus the brGDGT data was not used for either pH or MAT and will not be discussed further.

***Magnetic Susceptibility***

Magnetic susceptibility (MS), typically used as a measure of detrital sedimentation (Da Silva et al., 2015), varies throughout UDR 1A (Fig. 7) and generally correlates positively with sediment grain size. The highest MS values coincide with the colder phases, and MS values decrease within the warmer phases, as sediments grain size is generally finer.

*Basal and Lower Cold Phase (~308 – 339 mbs)*

MS values in the base of the lacustrine section (~332-339 mbs), which peak at 1046 SI, are the highest of any throughout the lake section, coinciding with the occurrence of coarse sand-pebble layers. The lower cold phase (~308-332 mbs) MS values range from -0.1 to 246 SI, with most peaks at ~150 SI. Although these values are high near the base of the phase, they decrease near the top.

*Lower Warm Phase (~255 – 308 mbs)*

The lower warm phase has varying MS values which are generally lower when compared to the previous interval, with values ranging from -1.5 to 148 SI.

*Upper Cold Phase (~235 – 255 mbs)*

The third interval exhibits an increase in MS values, ranging from -1.5 to 229 SI.

*Upper Warm Phase (~200 – 235 mbs)*

The fourth and upper warm phase has 4 peaks, the highest at 445 SI, but has lowest mean of MS values.

***X-ray Fluorescence (Zr counts, Ti/Al and Mg/Al count ratios)***

High Ti/Al ratios were used as a proxy for a higher proportion of coarse-grained detritus (Jiménez-Espejo et al., 2007; Ziegler et al., 2010), and high Mg/Al ratio values were used as a proxy for high precipitation rates (Jiménez-Espejo et al., 2007; Martín-Puertas et al., 2010), and like MS values, varies throughout UDR 1A (Fig. 8) and follow the general trend of sediment color and climatic phases. Zr counts were also used for comparison with MS, since it can be used as a proxy for heavy mineral content and grain size (Johnson, et al. 2021). Since high rates of coarse-grained sedimentation are to some extent dependent on the energy of the environment, and the amount of precipitation coming into the basin catchment area, Zr counts, Ti/Al and Mg/Al ratios results are integrated below.

The basal and lower cold phases exhibit the highest averages of Zr counts (4043.7) and highest average Ti/Al (64.4) and Mg/Al (0.06) ratios. Upwards through the core, averages for the warmer phases are generally lower and decrease upwards. The upper warm phase exhibits the lowest average of Zr counts (3526.7) and lowest average Ti/Al (36.04) and Mg/Al (0.04) ratios.

**DISCUSSION**

Here, I address the integration of the data in the context of the two glacial-interglacial cycles -- or the hemicycles identified through the pollen assemblages – the lower cool phase, lower warm phase, upper cool phase, and upper warm phase. This cyclic pattern is also apparent in other data collections such as charcoal concentrations, magnetic susceptibility, and sedimentology.

Paleo Lake Unaweep was created by a catastrophic landslide near the western canyon mouth that obstructed the path of the ancestral Gunnison River and led to impoundment (Soreghan et al., 2015; Harris 2023). The steep paleorelief (>1000 m) in the vicinity of the UDR1 coring site presumably promoted the predominance of mass-flow event beds documented by Harris (2023) throughout the cored stratigraphy. Superimposed on this stratigraphy is a climatic cyclicity consisting primarily of two glacial-interglacial cycles, as detailed below.

*Basal Core – (~332-339 mbs, "Warm" Climate State)*

On the basis on one sample that yielded palynomorphs in this basal-most 7 m interval, Harris (2023) interprets this interval as recording a series of turbidites preserving classic Bouma sequences, with coarse-grained (coarse sand to pebbles) bases and fine (fine sand to clay) caps. Given the recovery of pollen from only one sample, a definitive interpretation for paleoclimate in this section is elusive.

Although this interval exhibits a high raw count of 19 charcoal particles, i.e., charcoal concentrations for each sample not regarding weight, CHAR calculations did not reveal discrete fire events (Fig. 8), suggesting that the presence of charcoal in this section could reflect the newly formed paleolake's high-energy environment. High-energy environments have the potential to introduce secondary charcoal-- redeposited charcoal from previous fire events, or surface run-off charcoal from the surrounding drainage basin (Whitlock & Larsen, 2002)-- creating the illusion of "fake" fire events (Conedera et al., 2009). This may indicate a fire event occurring years or even decades before, supported by the high MS values suggesting high deposition of clastic content (Long et al. 1998; Beaty & Taylor, 2009).

*Lower Cool Phase – Glacial (~308 – 332 mbs)*

Similar to the basal core, sediments in the Lower Cool Phase comprise reddish-brown and ochre-colored graded beds (turbidites) 1-50 cm thick, with bases composed of very coarse sand to pebbles, and clay caps. Locally, convolute bedding and bioturbation affect the clay tops. These facies record high-energy deposition consistent with the particularly high relief that persisted early in the history of Unaweep paleolake.

Total and macro-CHAR averages were the lowest in this phase. Four peaks of raw charcoal counts were noted in four discrete depths; however, similar to the basal interval, none were flagged as potential fire events, likely reflecting the high-energy environment (Fig. 9). MS values, which are relatively high when compared to other phases and remain steady throughout the base of this phase, only decreasing halfway at depth (~325 mbs). High MS values are often attributed to high deposition of detrital sediments, and this high deposition could possibly introduce secondary charcoal. When compared to the other climate phases, the higher Zr counts and Ti/Al count ratios in this climate phase further suggest that the lacustrine environment was experiencing higher proportions of coarse-grained sediment influx. Coarser sediment influx is interpreted to reflect higher precipitation and runoff during this phase, also supported by the high Mg/Al count ratios.

Low CHAR averages and overall low presence of charcoal, coincide with this phase's climate interpretation from the pollen assemblages—a predominance of *Picea* and *Abies* and *Pinus*/*Picea*+*Abies* and low percentages of desert shrubs, indicating cold-wet climate conditions. This combination of conditions could have promoted vast vegetation growth but hindered fire occurrence (Moreno, 2004), by influencing and increasing the overall fuel and soil moisture, which is dependent, in part, on precipitation (Vinney, 1991; Nelson, 2000; Sharples, 2009).

*Lower Warm Phase-- Interglacial (~255 – 308 mbs)*

The prevalence of drab olive-gray sediment colors and generally finer-grained event beds (coarse sand to clay) sediment is interpreted to record less-oxygenated conditions consistent with warmer climate conditions (and water column), as also indicated by the pollen assemblages. Total and macro CHAR averages in this phase increase compared to previous phases and total CHAR calculations show one potential fire event (Fig. 8). Total and micro CHAR averages are higher compared to macro CHAR average, which could relate to one of the following: 1) Breakdown of macro charcoal particles during sediment transport in gravity flows, or 2) increased depositions of micro particles (micro-charcoal) owing to increases in local or regional fires (Clark et al. 1998; Gardner & Whitlock, 2001), in addition to 3) low macro-charcoal (which tends to travel shorter distances) indicating the occurrence of smaller, less-frequent fire events in the direct watershed (Ward & Hardy, 1991; Duffin et al., 2008). MS values, Zr counts, and Ti/Al ratio all decrease in this climate phase, reflecting overall finer grained detrital input, consistent with less runoff and drier conditions. A decrease in Mg/Al ratios and slight increase in percentages of desert shrub pollen similarly suggests warmer-drier conditions.

Previous studies have explored the relationship between climate and wildfire, finding that fire occurrence tends to increase during hot-dry climate conditions (Power et al., 2010; Han et al., 2016; Moreno et al., 2018; Lu et al., 2021). Anderson et al. (2020) focused on the southern Colorado Rockies, which are prevalent with *Abies*, *Picea*, and *Pinus* vegetation, similar to that of Unaweep Canyon. Anderson et al. (2020) noted that not only does fire occurrence tend to increase during the warmer-drier climate stages, but a change in vegetation also occurs, like the shift seen in Unaweep's lower cool phase into the lower warm phase. The increase in raw charcoal counts and CHAR in the lower warm phase, may have been caused by the warm and

dry climate conditions of this phase and the abundance of *Picea* and *Pinus* vegetation produced during the previous phase.

An important component of wildfire is the fuel available for combustion (Marlon, 2020). Hence, the vegetation type can affect wildfire activity, with forest species such as *Picea* and *Pinus* increasing flammability (Blarquez et al., 2015; Feurdean et al., 2017). The lower warm phase increase in charcoal presence and CHAR could have been caused by both the increase in wildfires due to warmer-drier climates and the abundance of *Picea* and *Pinus* vegetation accumulated during the lower cool phase. When keeping in mind that wildfire has great potential to disturb existing vegetation, the decrease of Picea and Pinus concentrations in this warm phase may have also been caused by wildfires killing or causing injury to these vegetation types (Blarquez et al. 2015; Minckley & Long, 2016; Calder et al. 2019).

*Upper Cool Phase-- Glacial (~235 – 255 mbs)*

Sedimentary facies within the upper cool phase are generally finer than those of the lower cool phase, comprising turbidites of fine to coarse sand that grade to clay caps. Additionally, they are less oxidized, exhibiting mostly ochre colors with multiple occurrences of olive gray colors (~236 – 238, 339, 247.5 – 248 mbs) in contrast to the reds of the lower phase. Although there is an increase in MS values, Zr counts, and Ti/Al ratios, these values are only slightly lower than those in the lower cold phase. We interpret that this decrease from the previous cold phase suggests that although proportions of coarse detrital input were higher in the upper cold phase compared to the warmer phases, general grain size decreased as the lake continued to fill with sediment over time. Climatic conditions appear overall similar to the lower cold phase, as high Mg/Al and relatively lower percentages of desert shrubs suggest pluvial conditions, while high concentrations of *Pinus*, *Picea* and *Abies* pollen suggest cold conditions. Charcoal counts are

higher in the drab-colored intervals, but the lack of any prominent peaks suggests a prevalence of secondary charcoal, representative of fire events that occurred years before, and consistent with the cold-wet conditions indicated by the pollen (Fig. 8).

*Upper Warm Phase-- Interglacial (~200 – 235 mbs)*

Sedimentology in the upper warm phase is similar to that recorded in the lower warm phase, with a prevalence of olive-gray, relatively fine-grained graded beds comprising predominantly very fine sand or silt grading to clay, and, less commonly, fine- to coarse sand grading to clay. The drab colors reflect less-oxygenated conditions consistent with the pollen evidence for warmer temperatures, and the finer grain sizes reflect less-energetic flows consistent with generally drier conditions. These interpretations are also consistent with the XRF data (Zr, Ti/Al, Mg/Al) in this phase, all of which exhibit the lowest values present within the core. Indeed, the highest averages of *Artemisia*/*Picea*, *Pinus*/*Picea+Abies* and desert shrubs in this interval indicate the warmest and driest conditions of the entire study interval. The high values of total CHAR and macro-CHAR indicate that fire events were more frequent, more intense, and closer in proximity to the Unaweep paleolake basin than in any other interval, with two potential fire events (Fig. 8). Insolation has been studied before as a powerful influence on paleofires (Daniau et al., 2013; Whitlock et al., 2007; Kappenberg et al., 2019), suggesting that an increase of solar radiation can enhance the frequency and intensity of fire events. Mean daily insolation patterns during the 1.34 – 1.41 Ma time span, determined at 38º N and 108 º W, coincide with potential fire events (Fig. 8). Warm interglacial phases were exposed to higher solar insolation and exhibit higher average CHAR.

**Comparisons with Other Studies**

Most paleofire studies are conducted on short (<10 m) and laminated sediment records, using a higher-resolution sampling scheme than the ~50 cm interval used in this study. However, approaches to sampling for and analysis of charcoal for paleofire interpretations vary within the research community (Conedera et al., 2009); indeed, some question the use of CharAnalysis, a diagnostic and analytical software for sediment charcoal analysis (Higuera et al., 2009), and CHAR (charcoal accumulation rates) for interpretation of fire histories (Finsinger et al., 2014; Graves et al. 2019; Galloway & Lindstorm, 2023).

There are no paleoclimate studies targeting the early Pleistocene from western Colorado or the greater area and, those that do exist are in regions not necessarily affected by the same climate regime. An important climate feature of the Pleistocene is its glacial-interglacial cycles, which led to great variability in hydroclimate in western North America (McGee, 2020). Allstadt et al., (2021) provided palynological data for the late Pliocene to early Pleistocene (c. 2.8-2.24 Ma) from a paleo-lake in Idaho, reporting wetter conditions during glacial periods. Staley et al. (2022) provided paleoclimate data for Stoneman Lake, Arizona, on the southwestern Colorado Plateau, suggesting that although pre-MPT glacials experienced lower moisture levels than glacials of the late Pleistocene, the southwestern U.S. experienced pluvial conditions during glacial phases. This pattern of increased pluvial conditions during glacials is seen in other intervals of the Pleistocene, and the Holocene, where greater moisture availability was observed due to an increase of precipitation or a decrease in evaporation, or in some cases a combination of both (Wendt, 2018).

In Unaweep Canyon specifically, the proposed climate conditions agree with previous studies focusing on climatic conditions during glacial-interglacial phases, including in studies

much closer in age (Allstadt et al., 2021) and studies closer in age and location (Staley et al., 2022).

## CONCLUSIONS

1) The UDR 1A core provides a new climate-paleofire record from the western U.S. during part of the early Pleistocene (~1.41 ± 0.19 - 1.34 ± 0.13 Ma)—an interval rarely captured.
2) Pollen assemblages identify two alternating "warm-cool" climate cycles, interpreted to be interglacial-glacial cycles. Low *Artemisia*/*Picea* and *Pinus*/*Picea*+*Abies* ratios and low desert shrubs percentages, indicating cold-wet climate conditions, characterized the glacial phases. In contrast, higher *Artemisia*/*Picea* and *Pinus*/*Picea*+*Abies* ratios and higher desert shrub percentages predominated during the interglacial phases, indicating warm-dry climate conditions. The younger "warm" cycle exhibits higher average ratios of *Artemisia*/*Picea* and *Pinus*/*Picea*+*Abies* than the older "warm" cycle, indicating that climate became warmer after each full cycle.
3) Total CHAR records indicate that Unaweep paleolake experienced a gradual increase of fire events through time, with the highest averages occurring during the younger interglacial phase. Macro-charcoal, often regarded as a good indicator of localized fires, also increases upward, possibly recording an increase in localized fires, an increase in fire intensity, or a combination of both.
4) Palynology and CHAR records suggest that fire frequency changed congruently with climate conditions. The fire record indicates that fire occurrence intensified during the 'warmer' intervals and diminished during the 'cooler' phases. Although there are

some chronological discrepancies, the data suggest that insolation during the interglacial phases exerted a significant influence on this increase of fire events.

**REFERENCES**


Adam, D. P., Sarna-Wojcicki, A. M., Rieck, H. J., Bradbury, J. P., Dean, W. E., & Forester, R. M. (1989). Tulelake, California: The last 3 million years. *Palaeogeography, Palaeoclimatology, Palaeoecology*, *72*, 89–103. https://doi.org/10.1016/0031-0182(89)90134-X

Adams, D. K., & Comrie, A. C. (1997). The North American Monsoon. *Bulletin of the American Meteorological Society*, *78*(10), 2197–2213. https://doi.org/10.1175/1520-0477(1997)078<2197:TNAM>2.0.CO;2

Ali, A. A., Higuera, P. E., Bergeron, Y., & Carcaillet, C. (2009). Comparing fire-history interpretations based on area, number and estimated volume of macroscopic charcoal in lake sediments. *Quaternary Research*, *72*(3), 462–468. https://doi.org/10.1016/j.yqres.2009.07.002

Allstädt, F. J., Koutsodendris, A., Appel, E., Rösler, W., Reichgelt, T., Kaboth-Bahr, S., Prokopenko, A. A., & Pross, J. (2021). Late Pliocene to early Pleistocene climate dynamics in western North America based on a new pollen record from paleo-Lake Idaho. *Palaeobiodiversity and Palaeoenvironments*, *101*(1), 177–195. https://doi.org/10.1007/s12549-020-00460-1

Anderson, R. S., Jiménez-Moreno, G., Belanger, M., & Briles, C. (2020). Fire history of the unique high-elevation Snowmastodon (Ziegler Reservoir) site during MIS 6–4, with comparisons of TII to TI in the southern Colorado Rockies. *Quaternary Science Reviews*, *232*, 106213. https://doi.org/10.1016/j.quascirev.2020.106213

Aslan, A., Karlstrom, K., Hood, W. C., Cole, R. D., Oesleby, T. W., Betton, C., Sandoval, M. M., Darling, A., Kelley, S., Hudson, A., Kaproth, B., Schoepfer, S., Benage, M., & Landman, R. (2008). River incision histories of the Black Canyon of the Gunnison and Unaweep Canyon: Interplay between late Cenozoic tectonism, climate change, and drainage integration in the

western Rocky Mountains. In R. G. Raynolds (Ed.), Roaming the Rocky Mountains and Environs: Geological Field Trips (Vol. 10, p. 0). Geological Society of America. https://doi.org/10.1130/2007.fld010(04)

Atwood, W. W., & Mather, K. F. (1912). The Evidence of Three Distinct Glacial Epochs in the Pleistocene History of the San Juan Mountains, Colorado. *The Journal of Geology*, *20*(5), 385–409. https://doi.org/10.1086/621985

Bajo, P., Drysdale, R. N., Woodhead, J. D., Hellstrom, J. C., Hodell, D., Ferretti, P., Voelker, A. H. L., Zanchetta, G., Rodrigues, T., Wolff, E., Tyler, J., Frisia, S., Spötl, C., & Fallick, A. E. (2020). Persistent influence of obliquity on ice age terminations since the Middle Pleistocene transition. *Science*, *367*(6483), 1235–1239. https://doi.org/10.1126/science.aaw1114

Balco, G., Soreghan, G. S., Sweet, D. E., Marra, K. R., & Bierman, P. R. (2013). Cosmogenic-nuclide burial ages for Pleistocene sedimentary fill in Unaweep Canyon, Colorado, USA. *Quaternary Geochronology*, *18*, 149–157. https://doi.org/10.1016/j.quageo.2013.02.002

Beaty, R. M., & Taylor, A. H. (2009). A 14-000 year sedimentary charcoal record of fire from the northern Sierra Nevada, Lake Tahoe Basin, California, USA. The Holocene, 19 (3), 347–358. https://doi.org/10.1177/0959683608101386

Beaudoin, A. B. (1986). Using *Picea*/*Pinus* Ratios from the Wilcox Pass Core, Jasper National Park, Alberta, to Investigate Holocene Timberline Fluctuations. *Géographie Physique et Quaternaire*, *40*(2), 145–152. https://doi.org/10.7202/032634ar

Berends, C. J., Köhler, P., Lourens, L. J., & Van De Wal, R. S. W. (2021). On the cause of the Mid-Pleistocene Transition. *Reviews of Geophysics*, *59*(2), e2020RG000727. https://doi.org/10.1029/2020RG000727

Bhattacharya, T., Tierney, J. E., Addison, J. A., & Murray, J. W. (2018). Ice-sheet modulation of deglacial North American monsoon intensification. *Nature Geoscience*, 11(11), 848–852. https://doi.org/10.1038/s41561-018-0220-7

Bigio, E., Swetnam, T. W., & Baisan, C. H. (2010). A comparison and integration of tree-ring and alluvial records of fire history at the Missionary Ridge Fire, Durango, Colorado, USA. *The Holocene*, 20(7), 1047–1061. https://doi.org/10.1177/0959683610369502

Blarquez, O., Ali, A. A., Girardin, M. P., Grondin, P., Fréchette, B., Bergeron, Y., & Hély, C. (2015). Regional paleofire regimes affected by non-uniform climate, vegetation and human drivers. Scientific Reports, 5(1), 13356. https://doi.org/10.1038/srep13356

Bowman, D. M. J. S., Balch, J. K., Artaxo, P., Bond, W. J., Carlson, J. M., Cochrane, M. A., D'Antonio, C. M., DeFries, R. S., Doyle, J. C., Harrison, S. P., Johnston, F. H., Keeley, J. E., Krawchuk, M. A., Kull, C. A., Marston, J. B., Moritz, M. A., Prentice, I. C., Roos, C. I., Scott, A. C., … Pyne, S. J. (2009). Fire in the Earth System. *Science*, *324*(5926), 481–484. https://doi.org/10.1126/science.1163886

Branson, F. A., Miller, R. F., & McQueen, I. S. (1976). Moisture Relationships in Twelve Northern Desert Shrub Communities Near Grand Junction, Colorado. *Ecology*, *57*(6), 1104–1124. https://doi.org/10.2307/1935039

Briles, C. E., Whitlock, C., & Meltzer, D. J. (2012). Last glacial–interglacial environments in the southern Rocky Mountains, USA and implications for Younger Dryas-age human occupation. *Quaternary Research*, *77*(1), 96–103. https://doi.org/10.1016/j.yqres.2011.10.002

Brown, K. J., Clark, J. S., Grimm, E. C., Donovan, J. J., Mueller, P. G., Hansen, B. C. S., & Stefanova, I. (2005). Fire cycles in North American interior grasslands and their relation to

prairie drought. *Proceedings of the National Academy of Sciences*, *102*(25), 8865–8870. https://doi.org/10.1073/pnas.0503621102

Calder, W. J., Stefanova, I., & Shuman, B. (2019). Climate–fire–vegetation interactions and the rise of novel landscape patterns in subalpine ecosystems, Colorado. Journal of Ecology, 107(4), 1689–1703. https://doi.org/10.1111/1365-2745.13138

Cannon, S. H., & DeGraff, J. (2009). The increasing wildfire and post-fire debris-flow threat in western USA, and implications for consequences of climate change. In K. Sassa & P. Canuti (Eds.), *Landslides – Disaster Risk Reduction* (pp. 177–190). Springer Berlin Heidelberg. https://doi.org/10.1007/978-3-540-69970-5_9

Chalk, T. B., Hain, M. P., Foster, G. L., Rohling, E. J., Sexton, P. F., Badger, M. P. S., Cherry, S. G., Hasenfratz, A. P., Haug, G. H., Jaccard, S. L., Martínez-García, A., Pälike, H., Pancost, R. D., & Wilson, P. A. (2017). Causes of ice age intensification across the Mid-Pleistocene Transition. *Proceedings of the National Academy of Sciences*, *114*(50), 13114–13119. https://doi.org/10.1073/pnas.1702143114

Clark, J. S., Lynch, J., Stocks, B. J., & Goldammer, J. G. (1998). Relationships between charcoal particles in air and sediments in west-central Siberia. *The Holocene*, *8*(1), 19–29. https://doi.org/10.1191/095968398672501165

Cole, R. D., & Sexton, J. L. (1981). Pleistocene surficial deposits of the Grand Mesa area, Colorado. Western Slope (Western Colorado), 121–126. https://doi.org/10.56577/FFC-32.121

Cole, R. D., & Young, R. G. (1983). Evidence for glaciation in Unaweep Canyon, Mesa County, Colorado. In Averett W.R. (Ed.), Northern Paradox Basin – *Uncompahgre Uplift (Grand*

*Junction Geological Society Field Trip Guidebook): Grand Junction, Colorado, Grand Junction Geological Society,* p. 73-80.

Collinson, M. E., Steart, D. C., Scott, A. C., Glasspool, I. J., & Hooker, J. J. (2007). Episodic fire, runoff and deposition at the Palaeocene–Eocene boundary. *Journal of the Geological Society*, *164*(1), 87–97. https://doi.org/10.1144/0016-76492005-185

Conedera, M., Tinner, W., Neff, C., Meurer, M., Dickens, A. F., & Krebs, P. (2009). Reconstructing past fire regimes: Methods, applications, and relevance to fire management and conservation. *Quaternary Science Reviews*, *28*(5–6), 555–576. https://doi.org/10.1016/j.quascirev.2008.11.005

Da, J., Zhang, Y. G., Li, G., Meng, X., & Ji, J. (2019). Low $CO_2$ levels of the entire Pleistocene epoch. *Nature Communications*, *10*(1), 4342. https://doi.org/10.1038/s41467-019-12357-5

Daniau, A.-L., Sánchez-Goñi, M. F., Beaufort, L., Laggoun-Défarge, F., Loutre, M.-F., & Duprat, J. (2007). Dansgaard–Oeschger climatic variability revealed by fire emissions in southwestern Iberia. *Quaternary Science Reviews*, *26*(9–10), 1369–1383. https://doi.org/10.1016/j.quascirev.2007.02.005

Daniau, A.-L., Harrison, S. P., & Bartlein, P. J. (2010). Fire regimes during the Last Glacial. Quaternary Science Reviews, 29(21–22), 2918–2930. https://doi.org/10.1016/j.quascirev.2009.11.008

Daniau, A.-L., Sánchez Goñi, M. F., Martinez, P., Urrego, D. H., Bout-Roumazeilles, V., Desprat, S., & Marlon, J. R. (2013). Orbital-scale climate forcing of grassland burning in southern Africa. *Proceedings of the National Academy of Sciences*, *110*(13), 5069–5073. https://doi.org/10.1073/pnas.1214292110

Da Silva, A. C., Whalen, M. T., Hladil, J., Chadimova, L., Chen, D., Spassov, S., Boulvain, F., & Devleeschouwer, X. (2015). Magnetic susceptibility application: A window onto ancient environments and climatic variations: foreword. Geological Society, London, Special Publications, 414(1), 1–13. https://doi.org/10.1144/SP414.12

Davis, O. K. (1998). Palynological evidence for vegetation cycles in a 1.5 million year pollen record from the Great Salt Lake, Utah, USA. *Palaeogeography, Palaeoclimatology, Palaeoecology*, *138*(1–4), 175–185. https://doi.org/10.1016/S0031-0182(97)00105-3

De Jonge, C., Hopmans, E. C., Zell, C. I., Kim, J.-H., Schouten, S., & Sinninghe Damsté, J. S. (2014). Occurrence and abundance of 6-methyl branched glycerol dialkyl glycerol tetraethers in soils: Implications for palaeoclimate reconstruction. *Geochimica et Cosmochimica Acta*, *141*, 97–112. https://doi.org/10.1016/j.gca.2014.06.013

de la Vega, E., Chalk, T. B., Wilson, P. A., Bysani, R., and Foster, G. L.: Atmospheric $CO_2$ during the Mid-Piacenzian Warm Period and the M2 glaciation., EGU General Assembly 2020, Online, 4–8 May 2020, EGU 2020-11480. https://doi.org/10.5194/egusphere-egu2020-11480

Dilts, T. E., Weisberg, P. J., Dencker, C. M., & Chambers, J. C. (2015). Functionally relevant climate variables for arid lands: A climatic water deficit approach for modelling desert shrub distributions. *Journal of Biogeography*, *42*(10), 1986–1997. https://doi.org/10.1111/jbi.12561

Douglas, M. W., Maddox, R. A., Howard, K., & Reyes, S. (1993). The Mexican Monsoon. *Journal of Climate*, *6*(8), 1665–1677. https://doi.org/10.1175/1520-0442(1993)006<1665:TMM>2.0.CO;2

Duffin, K. I., Gillson, L., & Willis, K. J. (2008). Testing the sensitivity of charcoal as an indicator of fire events in savanna environments: Quantitative predictions of fire proximity, area and intensity. *The Holocene*, *18*(2), 279–291. https://doi.org/10.1177/0959683607086766

Feurdean, A., Veski, S., Florescu, G., Vannière, B., Pfeiffer, M., O'Hara, R. B., Stivrins, N., Amon, L., Heinsalu, A., Vassiljev, J., & Hickler, T. (2017). Broadleaf deciduous forest counterbalanced the direct effect of climate on Holocene fire regime in hemiboreal/boreal region (NE Europe). Quaternary Science Reviews, 169, 378–390. https://doi.org/10.1016/j.quascirev.2017.05.024

Finsinger, W., Kelly, R., Fevre, J., & Magyari, E. K. (2014). A guide to screening charcoal peaks in macrocharcoal-area records for fire-episode reconstructions. *The Holocene*, *24*(8), 1002–1008. https://doi.org/10.1177/0959683614534737

Fritz, S. C. (1996). Paleolimnological records of climatic change in North America. *Limnology and Oceanography*, *41*(5), 882–889. https://doi.org/10.4319/lo.1996.41.5.0882

Galloway, J. M., & Lindström, S. (2023). Wildfire in the geological record: Application of Quaternary methods to deep time studies. *Evolving Earth*, *1*, 100025. https://doi.org/10.1016/j.eve.2023.100025

Gardner, J. J., & Whitlock, C. (2001). Charcoal accumulation following a recent fire in the Cascade Range, northwestern USA, and its relevance for fire-history studies. *The Holocene*, *11*(5), 541–549. https://doi.org/10.1191/095968301680223495

Gillam, M. L. (1998). Late Cenozoic Geology and Soils of the Lower Animas River Valley, Colorado and New Mexico: PhD Thesis. University of Colorado, 590 p.

Graves, B. P., Ralph, T. J., Hesse, P. P., Westaway, K. E., Kobayashi, T., Gadd, P. S., & Mazumder, D. (2019). Macro-charcoal accumulation in floodplain wetlands: Problems and prospects for reconstruction of fire regimes and environmental conditions. *PLOS ONE*, *14*(10), e0224011. https://doi.org/10.1371/journal.pone.0224011

Groot, J. J. (1991). Palynological evidence for late Miocene, Pliocene and early Pleistocene climate changes in the middle U.S. Atlantic Coastal Plain. *Quaternary Science Reviews*, *10*(2–3), 147–162. https://doi.org/10.1016/0277-3791(91)90015-M

Han, Y. M., Peteet, D. M., Arimoto, R., Cao, J. J., An, Z. S., Sritrairat, S., & Yan, B. Z. (2016). Climate and Fuel Controls on North American Paleofires: Smoldering to Flaming in the Late-glacial-Holocene Transition. *Scientific Reports*, *6*(1), 20719. https://doi.org/10.1038/srep20719

Harris, B. (2023). Sedimentological Study of an Early Pleistocene Upland Lake Core, Unaweep Canyon, Colorado: M.S. Thesis, University of Oklahoma, 186 p.

Herbert, T. D. (2023). The Mid-Pleistocene Climate Transition. *Annual Review of Earth and Planetary Sciences*, *51*(1), 389–418. https://doi.org/10.1146/annurev-earth-032320-104209

Higuera, P., Peters, M., Brubaker, L., & Gavin, D. (2007). Understanding the origin and analysis of sediment-charcoal records with a simulation model. *Quaternary Science Reviews*, *26*(13–14), 1790–1809. https://doi.org/10.1016/j.quascirev.2007.03.010

Higuera, P. E., Brubaker, L. B., Anderson, P. M., Hu, F. S., & Brown, T. A. (2009). Vegetation mediated the impacts of postglacial climate change on fire regimes in the south-central Brooks Range, Alaska. *Ecological Monographs*, *79*(2), 201–219. https://doi.org/10.1890/07-2019.1

Huang, Z., Ma, C., Chyi, S., Tang, L., & Zhao, L. (2020). Paleofire, Vegetation, and Climate Reconstructions of the Middle to Late Holocene From Lacustrine Sediments of the Toushe Basin, Taiwan. *Geophysical Research Letters*, *47*(20), e2020GL090401. https://doi.org/10.1029/2020GL090401

Iglesias, V., Yospin, G. I., & Whitlock, C. (2015). Reconstruction of fire regimes through integrated paleoecological proxy data and ecological modeling. *Frontiers in Plant Science*, *5*. https://doi.org/10.3389/fpls.2014.00785

Jasper, A., Pozzebon–Silva, Â., Siqueira Carniere, J., & Uhl, D. (2021). Palaeozoic and Mesozoic palaeo–wildfires: An overview on advances in the 21st Century. *Journal of Palaeosciences*, *70*((1-2)), 159–172. https://doi.org/10.54991/jop.2021.13

Jiménez-Espejo, F. J., Martínez-Ruiz, F., Finlayson, C., Paytan, A., Sakamoto, T., Ortega-Huertas, M., Finlayson, G., Iijima, K., Gallego-Torres, D., & Fa, D. (2007). Climate forcing and Neanderthal extinction in Southern Iberia: Insights from a multiproxy marine record. Quaternary Science Reviews, 26(7–8), 836–852. https://doi.org/10.1016/j.quascirev.2006.12.013

Jiménez-Moreno, G., Fauquette, S., & Suc, J. (2008). Vegetation, climate and palaeoaltitude reconstructions of the Eastern Alps during the Miocene based on pollen records from Austria, Central Europe. *Journal of Biogeography*, *35*(9), 1638–1649. https://doi.org/10.1111/j.1365-2699.2008.01911.x

Jimenez-Moreno, G., Anderson, R. S., Atudorei, V., & Toney, J. L. (2011). A high-resolution record of climate, vegetation, and fire in the mixed conifer forest of northern Colorado, USA. *Geological Society of America Bulletin*, *123*(1–2), 240–254. https://doi.org/10.1130/B30240.1

Jiménez-Moreno, G., Anderson, R. S., Markgraf, V., Staley, S. E., & Fawcett, P. J. (2023). Environmental and climate evolution in the Southwest USA since the last interglacial deduced from the pollen record from Stoneman lake, Arizona. *Quaternary Science Reviews*, *300*, 107883. https://doi.org/10.1016/j.quascirev.2022.107883

Jenkins, S. E., Hull Sieg, C., Anderson, D. E., Kaufman, D. S., & Pearthree, P. A. (2011). Late Holocene geomorphic record of fire in ponderosa pine and mixed-conifer forests, Kendrick Mountain, northern Arizona, USA. *International Journal of Wildland Fire*, *20*(1), 125. https://doi.org/10.1071/WF09093

Johnson, B. G., Jiménez-Moreno, G., Eppes, M. C., Diemer, J. A., & Stone, J. R. (2013). A multiproxy record of postglacial climate variability from a shallowing, 12-m deep sub-alpine bog in the southeastern San Juan Mountains of Colorado, USA. *The Holocene*, *23*(7), 1028–1038. https://doi.org/10.1177/0959683613479682

Johnson, B., Gillam, M., & Beeton, J. (2017). Glaciations of the San Juan Mountains: A review of work since Atwood and Mather. *The Geology of the Ouray-Silverton Area*, 195–204. https://doi.org/10.56577/FFC-68.195

Jolly, W. M., Cochrane, M. A., Freeborn, P. H., Holden, Z. A., Brown, T. J., Williamson, G. J., & Bowman, D. M. J. S. (2015). Climate-induced variations in global wildfire danger from 1979 to 2013. *Nature Communications*, *6*(1), 7537. https://doi.org/10.1038/ncomms8537

Jurvélius, M. (2004). Health & Protection | Forest Fires (Prediction, Prevention, Preparedness and Suppression). In *Encyclopedia of Forest Sciences* (pp. 334–339). Elsevier. https://doi.org/10.1016/B0-12-145160-7/00277-5

Kaplan, S.A., 2006. Revealing Unaweep Canyon: The Late Cenozoic Exhumation History of Unaweep Canyon as Recorded by Gravels in Gateway, Colorado: M.S. Thesis, University of Oklahoma 52 p.

Kappenberg, A., Lehndorff, E., Pickarski, N., Litt, T., & Amelung, W. (2019). Solar controls of fire events during the past 600,000 years. *Quaternary Science Reviews*, *208*, 97–104. https://doi.org/10.1016/j.quascirev.2019.02.008

Kaufman, D., McKay, N., Routson, C., Erb, M., Davis, B., Heiri, O., Jaccard, S., Tierney, J., Dätwyler, C., Axford, Y., Brussel, T., Cartapanis, O., Chase, B., Dawson, A., De Vernal, A., Engels, S., Jonkers, L., Marsicek, J., Moffa-Sánchez, P., … Zhilich, S. (2020). A global database of Holocene paleotemperature records. *Scientific Data*, *7*(1), 115. https://doi.org/10.1038/s41597-020-0445-3

Kim, Y., Yi, S., Jun, C.-P., Saavedra-Pellitero, M., Lee, G.-S., & Kim, G. Y. (2023). Palynological implications for the paleoclimate and paleoceanographic reconstruction of the East Sea since the early Pleistocene at IODP site U1430. *Quaternary Science Reviews*, *315*, 108252. https://doi.org/10.1016/j.quascirev.2023.108252

Kolb, P. F., & Robberecht, R. (1996). *Pinus ponderosa* Seedling Establishment and the Influence of Competition with the Bunchgrass Agropyron spicatum. International Journal of Plant Sciences, 157(4), 509–515. http://www.jstor.org/stable/2475256

Legrain, E., Parrenin, F., & Capron, E. (2023). A gradual change is more likely to have caused the Mid-Pleistocene Transition than an abrupt event. *Communications Earth & Environment*, *4*(1), 90. https://doi.org/10.1038/s43247-023-00754-0

Leonard, E. M. (1984). Late Pleistocene Equilibrium-Line Altitudes and Modern Snow Accumulation Patterns, San Juan Mountains, Colorado, U.S.A. *Arctic and Alpine Research*, *16*(1), 65. https://doi.org/10.2307/1551173

Leonard, E. M. (1989). Climatic Change in the Colorado Rocky Mountains: Estimates Based on Modern Climate at Late Pleistocene Equilibrium Lines. *Arctic and Alpine Research*, *21*(3), 245. https://doi.org/10.2307/1551563

Liu, Y., L. Goodrick, S., & A. Stanturf, J. (2013). Future U.S. wildfire potential trends projected using a dynamically downscaled climate change scenario. *Forest Ecology and Management*, *294*, 120–135. https://doi.org/10.1016/j.foreco.2012.06.049

Lohman, S. W. (1981). Ancient drainage changes in and south of Unaweep Canyon, southwestern Colorado. *Western Slope (Western Colorado)*, 137–144. https://doi.org/10.56577/FFC-32.137

Long, C. J., Whitlock, C., Bartlein, P. J., & Millspaugh, S. H. (1998). A 9000-year fire history from the Oregon Coast Range, based on a high-resolution charcoal study. *Canadian Journal of Forest Research*, *28*(5), 774–787. https://doi.org/10.1139/x98-051

Lu, M., Ikejiri, T., & Lu, Y. (2021). A synthesis of the Devonian wildfire record: Implications for paleogeography, fossil flora, and paleoclimate. Palaeogeography, Palaeoclimatology, Palaeoecology, 571, 110321. https://doi.org/10.1016/j.palaeo.2021.110321

Marchetti, D. W., Harris, M. S., Bailey, C. M., Cerling, T. E., & Bergman, S. (2011). Timing of glaciation and last glacial maximum paleoclimate estimates from the Fish Lake Plateau, Utah. *Quaternary Research*, *75*(1), 183–195. https://doi.org/10.1016/j.yqres.2010.09.009

Marlon, J. R., Bartlein, P. J., Carcaillet, C., Gavin, D. G., Harrison, S. P., Higuera, P. E., Joos, F., Power, M. J., & Prentice, I. C. (2008). Climate and human influences on global biomass burning over the past two millennia. *Nature Geoscience*, *1*(10), 697–702. https://doi.org/10.1038/ngeo313

Marlon, J. R., Bartlein, P. J., Daniau, A.-L., Harrison, S. P., Maezumi, S. Y., Power, M. J., Tinner, W., & Vanniére, B. (2013). Global biomass burning: A synthesis and review of Holocene paleofire records and their controls. *Quaternary Science Reviews*, *65*, 5–25. https://doi.org/10.1016/j.quascirev.2012.11.029

Marlon, J. R. (2020). What the past can say about the present and future of fire. *Quaternary Research*, *96*, 66–87. https://doi.org/10.1017/qua.2020.48

Martín-Puertas, C., Jiménez-Espejo, F., Martínez-Ruiz, F., Nieto-Moreno, V., Rodrigo, M., Mata, M. P., & Valero-Garcés, B. L. (2010). Late Holocene climate variability in the southwestern Mediterranean region: An integrated marine and terrestrial geochemical approach. https://doi.org/10.5194/cpd-6-1655-2010

Marra, K.R. (2008). Late Cenozoic Geomorphic and Climatic Evolution of the Northeastern Colorado Plateau as Recorded by Plio-Pleistocene Sediment Fill in Unaweep Canyon, Colorado: M.S. Thesis, University of Oklahoma 160 p.

Maslin, M. A., Li, X. S., Loutre, M.-F., & Berger, A. (1998). The Contribution of Orbital Forcing to the Progressive Intensification of Northern Hemisphere Glaciation. *Quaternary Science Reviews*, *17*(4–5), 411–426. https://doi.org/10.1016/S0277-3791(97)00047-4

McGee, D. (2020). Glacial–Interglacial Precipitation Changes. Annual Review of Marine Science, 12(1), 525–557. https://doi.org/10.1146/annurev-marine-010419-010859

Milliman, J. D., & Syvitski, J. P. M. (1992). Geomorphic/Tectonic Control of Sediment Discharge to the Ocean: The Importance of Small Mountainous Rivers. The Journal of Geology, 100(5), 525–544. http://www.jstor.org/stable/30068527

Minckley, T. A., & Long, C. J. (2016). Paleofire severity and vegetation change in the Cascade Range, Oregon, USA. Quaternary Research, 85(2), 211–217. https://doi.org/10.1016/j.yqres.2015.12.010

Mishra, P. K. (2023). Lake Sediments and Climate Studies. In P. K. Mishra, *The Application of Lake Sediments for Climate Studies* (pp. 1–13). Springer International Publishing. https://doi.org/10.1007/978-3-031-34709-2_1

Mogen, C. T. (2018) The Paleoecology and Fire History from Crater Lake, Colorado: The Last 1000 Years: M.S. Thesis, Northern Arizona University 123 p.

Moreno, P. I. (2004). Millennial-scale climate variability in northwest Patagonia over the last 15,000 yrs. *Journal of Quaternary Science*, 19(1), 35–47. https://doi.org/10.1002/jqs.813

Moreno, P. I., Videla, J., Valero-Garcés, B., Alloway, B. V., & Heusser, L. E. (2018). A continuous record of vegetation, fire-regime and climatic changes in northwestern Patagonia spanning the last 25,000 years. *Quaternary Science Reviews*, 198, 15–36. https://doi.org/10.1016/j.quascirev.2018.08.013

Nelson Jr, R. M. (2000). Prediction of diurnal change in 10-h fuel stick moisture content. *Canadian Journal of Forest Research*, 30(7), 1071–1087. https://doi.org/10.1139/x00-032

Oster, J. L., Ibarra, D. E., Winnick, M. J., & Maher, K. (2015). Steering of westerly storms over western North America at the Last Glacial Maximum. *Nature Geoscience*, *8*(3), 201–205. https://doi.org/10.1038/ngeo2365

Otterman, J., & Chou, M.-D. (1992). Simulation of desert-scrub growth: A forcing to warmer and more pluvial climate. *Advances in Atmospheric Sciences*, *9*(4), 441–450. https://doi.org/10.1007/BF02677076

Patterson, A., Behm, M., Chwatal, W., Flores-Orozco, A., Wang, Y., & Soreghan, G. S. (2021). Seismic Reflection and Electrical Resistivity Imaging Support Pre-Quaternary Glaciation in the Rocky Mountains (Unaweep Canyon, Colorado). *Geophysical Research Letters*, *48*(18), e2021GL094706. https://doi.org/10.1029/2021GL094706

Peaple, M. D., Bhattacharya, T., Lowenstein, T. K., McGee, D., Olson, K. J., Stroup, J. S., Tierney, J. E., & Feakins, S. J. (2022). Biomarker and pollen evidence for Late Pleistocene pluvials in the Mojave Desert. *Paleoceanography and Paleoclimatology*, *37*(10), e2022PA004471. https://doi.org/10.1029/2022PA004471

Pierce, J. L., Meyer, G. A., & Timothy Jull, A. J. (2004). Fire-induced erosion and millennial-scale climate change in northern ponderosa pine forests. *Nature*, *432*(7013), 87–90. https://doi.org/10.1038/nature03058

Power, M. J., Marlon, J., Ortiz, N., Bartlein, P. J., Harrison, S. P., Mayle, F. E., Ballouche, A., Bradshaw, R. H. W., Carcaillet, C., Cordova, C., Mooney, S., Moreno, P. I., Prentice, I. C., Thonicke, K., Tinner, W., Whitlock, C., Zhang, Y., Zhao, Y., Ali, A. A., … Zhang, J. H. (2008). Changes in fire regimes since the Last Glacial Maximum: An assessment based on a global synthesis and analysis of charcoal data. *Climate Dynamics*, *30*(7–8), 887–907. https://doi.org/10.1007/s00382-007-0334-x

Power, M. J., Bush, M., Behling, H., Horn, S., Mayle, F., & Urrego, D. (2010). Paleofire activity in tropical America during the last 21 ka: A regional synthesis based on sedimentary charcoal. *PAGES News*, 18(2), 73–75. https://doi.org/10.22498/pages.18.2.73

Raymo, M. E., Lisiecki, L. E., & Nisancioglu, K. H. (2006). Plio-Pleistocene Ice Volume, Antarctic Climate, and the Global δ $^{18}$ O Record. *Science*, *313*(5786), 492–495. https://doi.org/10.1126/science.1123296

Richmond, G.M., (1962) Quaternary stratigraphy of the La Sal Mountains, Utah: U.S. Geological Survey Professional Paper 324, 135 p.

Richmond, G. (1986). Stratigraphy and correlation of glacial deposits of the Rocky Mountains, the Colorado Plateau and the ranges of the Great Basin. *Quaternary Science Reviews*, *5*, 99–127. https://doi.org/10.1016/S0277-3791(86)80013-0

Richmond G. M. & Fullerton, D.S. (1986) Summation of quaternary glaciations in the United States of America, *Quaternary Science Reviews*, Volume 5, p. 183-196, https://doi.org/10.1016/0277-3791(86)90184-8.

Riley, K. L., & Loehman, R. A. (2016). Mid-21st-century climate changes increase predicted fire occurrence and fire season length, Northern Rocky Mountains, United States. *Ecosphere*, *7*(11), e01543. https://doi.org/10.1002/ecs2.1543

Roos, C. I., & Swetnam, T. W. (2012). A 1416-year reconstruction of annual, multidecadal, and centennial variability in area burned for ponderosa pine forests of the southern Colorado Plateau region, Southwest USA. *The Holocene*, *22*(3), 281–290. https://doi.org/10.1177/0959683611423694

Ruggieri, E., Herbert, T., Lawrence, K. T., & Lawrence, C. E. (2009). Change point method for detecting regime shifts in paleoclimatic time series: Application to $\delta^{18}$ O time series of the Plio-Pleistocene. *Paleoceanography*, *24*(1), 2007PA001568. https://doi.org/10.1029/2007PA001568

Sánchez Goñi, M. F., Desprat, S., Daniau, A.-L., Bassinot, F. C., Polanco-Martínez, J. M., Harrison, S. P., Allen, J. R. M., Anderson, R. S., Behling, H., Bonnefille, R., Burjachs, F., Carrión, J. S., Cheddadi, R., Clark, J. S., Combourieu-Nebout, N., Mustaphi, Colin. J. C., Debusk, G. H., Dupont, L. M., Finch, J. M., … Yamamoto, M. (2017). The ACER pollen and charcoal database: A global resource to document vegetation and fire response to abrupt climate changes during the last glacial period. *Earth System Science Data*, *9*(2), 679–695. https://doi.org/10.5194/essd-9-679-2017

Schoennagel, T., Balch, J. K., Brenkert-Smith, H., Dennison, P. E., Harvey, B. J., Krawchuk, M. A., Mietkiewicz, N., Morgan, P., Moritz, M. A., Rasker, R., Turner, M. G., & Whitlock, C. (2017). Adapt to more wildfire in western North American forests as climate changes. *Proceedings of the National Academy of Sciences*, *114*(18), 4582–4590. https://doi.org/10.1073/pnas.1617464114

Schouten, S., Hopmans, E. C., & Sinninghe Damsté, J. S. (2013). The organic geochemistry of glycerol dialkyl glycerol tetraether lipids: A review. *Organic Geochemistry*, *54*, 19–61. https://doi.org/10.1016/j.orggeochem.2012.09.006

Sharples, J. J., McRae, R. H. D., Weber, R. O., & Gill, A. M. (2009). A simple index for assessing fuel moisture content. Environmental Modelling & Software, 24(5), 637–646. https://doi.org/10.1016/j.envsoft.2008.10.012

Sinnock, S. (1978). Geomorphology of the Uncompahgre Plateau and Grand Valley, western Colorado, U.S.A. (Ph.D. dissertation): West Lafayette, Indiana, Purdue University, p. 196

Soreghan, G., Sweet, D., Marra, K., Eble, C., Soreghan, M., Elmore, R., Kaplan, S., Blum, M. (2007). An exhumed late Paleozoic canyon in the Rocky Mountains.

Journal of Geology 115, 473e481.

Soreghan, G.S., Soreghan, M. J., Poulsen, C.J., Young, R. A., Eble, C. F., Sweet, D. E., & Davogustto, O. C. (2008). Anomalous cold in the Pangaean tropics. *Geology*, 36 (8): 659–662. https://doi-org.ezproxy.lib.ou.edu/10.1130/G24822A.1

Soreghan, G. S., Sweet, D. E., & Heavens, N. G. (2014). Upland Glaciation in Tropical Pangaea: Geologic Evidence and Implications for Late Paleozoic Climate Modeling. The Journal of Geology, 122(2), 137–163. https://doi.org/10.1086/675255

Soreghan, G. S., Sweet, D. E., Thomson, S. N., Kaplan, S. A., Marra, K. R., Balco, G., & Eccles, T. M. (2015). Geology of Unaweep Canyon and its role in the drainage evolution of the northern Colorado Plateau. Geosphere, 11(2), 320–341. https://doi.org/10.1130/GES01112.1

Sosdian, S., & Rosenthal, Y. (2009). Deep-Sea Temperature and Ice Volume Changes Across the Pliocene-Pleistocene Climate Transitions. *Science*, *325*(5938), 306–310. https://doi.org/10.1126/science.1169938

Staley, S. E., Fawcett, P. J., Anderson, R. S., & Jiménez-Moreno, G. (2022). Early Pleistocene–to–present paleoclimate archive for the American Southwest from Stoneman Lake, Arizona, USA. *GSA Bulletin*, *134*(3–4), 791–814. https://doi.org/10.1130/B36038.1

Sun, Y., Yin, Q., Crucifix, M., Clemens, S. C., Araya-Melo, P., Liu, W., Qiang, X., Liu, Q., Zhao, H., Liang, L., Chen, H., Li, Y., Zhang, L., Dong, G., Li, M., Zhou, W., Berger, A., & An, Z. (2019). Diverse manifestations of the mid-Pleistocene climate transition. *Nature Communications*, *10*(1), 352. https://doi.org/10.1038/s41467-018-08257-9

Syvitski, J. P. M. (2003). Sediment fluxes and rates of sedimentation. In Sedimentology (pp. 980–992). Springer Netherlands. https://doi.org/10.1007/978-1-4020-3609-5_180

Wang, Y., Momohara, A., Ito, A., Fukushima, T., & Huang, Y.-J. (2018). Warm climate under high CO2 level in the early Pleistocene based on a leaf fossil assemblage in central Japan. *Review of Palaeobotany and Palynology*, *258*, 146–153. https://doi.org/10.1016/j.revpalbo.2018.08.001

Ward, D. E., & Hardy, C. C. (1991). Smoke emissions from wildland fires. *Environment International*, *17*(2–3), 117–134. https://doi.org/10.1016/0160-4120(91)90095-8

Wardle, P. (1968). Engelmann Spruce (*Picea Engelmannii* Engel.) at Its Upper Limits on the Front Range, Colorado. *Ecology*, *49*(3), 483–495. https://doi.org/10.2307/1934115

Weijers, J. W. H., Schouten, S., Sluijs, A., Brinkhuis, H., & Sinninghe Damsté, J. S. (2007). Warm arctic continents during the Palaeocene–Eocene thermal maximum. *Earth and Planetary Science Letters*, *261*(1–2), 230–238. https://doi.org/10.1016/j.epsl.2007.06.033

Wendt, K. A., Dublyansky, Y. V., Moseley, G. E., Edwards, R. L., Cheng, H., & Spötl, C. (2018). Moisture availability in the southwest United States over the last three glacial-interglacial cycles. Science Advances, 4(10), eaau1375. https://doi.org/10.1126/sciadv.aau1375

Westerling, A. L., Hidalgo, H. G., Cayan, D. R., & Swetnam, T. W. (2006). Warming and earlier spring increase western U.S. forest wildfire activity. *Science*, *313*(5789), 940–943. https://doi.org/10.1126/science.1128834

Whitlock, C., & Millspaugh, S. H. (1996). Testing the assumptions of fire-history studies: An examination of modern charcoal accumulation in Yellowstone National Park, USA. *The Holocene*, *6*(1), 7–15. https://doi.org/10.1177/095968369600600102

Whitlock, C., & Larsen, C. (2002). Charcoal as a Fire Proxy. In J. P. Smol, H. J. B. Birks, W. M. Last, R. S. Bradley, & K. Alverson (Eds.), *Tracking Environmental Change Using Lake Sediments* (Vol. 3, pp. 75–97). Springer Netherlands. https://doi.org/10.1007/0-306-47668-1_5

Whitlock, C., Moreno, P. I., & Bartlein, P. (2007). Climatic controls of Holocene fire patterns in southern South America. *Quaternary Research*, *68*(1), 28–36. https://doi.org/10.1016/j.yqres.2007.01.012

Willeit, M., Ganopolski, A., Calov, R., & Brovkin, V. (2019). Mid-Pleistocene transition in glacial cycles explained by declining $CO_2$ and regolith removal. *Science Advances*, *5*(4), eaav7337. https://doi.org/10.1126/sciadv.aav7337

Yamamoto, M., Clemens, S. C., Seki, O., Tsuchiya, Y., Huang, Y., O'ishi, R., & Abe-Ouchi, A. (2022). Increased interglacial atmospheric CO2 levels followed the mid-Pleistocene Transition. *Nature Geoscience*, *15*(4), 307–313. https://doi.org/10.1038/s41561-022-00918-1

Yan, Y., Kurbatov, A. V., Mayewski, P. A., Shackleton, S., & Higgins, J. A. (2023). Early Pleistocene East Antarctic temperature in phase with local insolation. *Nature Geoscience*, *16*(1), 50–55. https://doi.org/10.1038/s41561-022-01095-x

Yeend, W. E., 1969, Quaternary geology of the Grand and Battlement Mesas area, Colorado: U.S. Geological Survey Professional Paper 617, p. 50

Young, J. W. (1983). Vegetation Zones of Western Colorado – Eastern Utah. In Averett W.R. (Ed.), Northern Paradox Basin – *Uncompahgre Uplift (Grand Junction Geological Society Field Trip Guidebook): Grand Junction, Colorado, Grand Junction Geological Society, p. 73-80.*

Ziegler, M., Lourens, L. J., Tuenter, E., & Reichart, G.-J. (2010). High Arabian Sea productivity conditions during MIS 13 – odd monsoon event or intensified overturning circulation at the end of the Mid-Pleistocene transition? Climate of the Past, 6(1), 63–76. https://doi.org/10.5194/cp-6-63-2010

Zhao, L., Lu, H., Wang, H., Zhang, H., Lei, F., & Tang, L. (2023). Paleofire dynamics in response to climate change during late Miocene derived from microcharcoal records in the Weihe Basin. *Quaternary International*, *671*, 44–51. https://doi.org/10.1016/j.quaint.2023.08.010

Zimmerman, S. R. H., & Wahl, D. B. (2020). Holocene paleoclimate change in the western US: The importance of chronology in discerning patterns and drivers. *Quaternary Science Reviews*, *246*, 106487. https://doi.org/10.1016/j.quascirev.2020.106487

Zolitschka, B., & Enters, D. (2009). Lacustrine Sediments. In V. Gornitz (Ed.), *Encyclopedia of Paleoclimatology and Ancient Environments* (pp. 486–488). Springer Netherlands. https://doi.org/10.1007/978-1-4020-4411-3_120

**TABLE 1 CORE DRILLING WELL SITE LOCATIONS, UNAWEEP CANYON, COLORADO**

| Well Site Name | Latitude, Longitude | Total Drilling Depth (mbs) | Total Destructive Drilling (mbs) | Percentage of Recovered Lacustrine Interval | Basement Reached? | Basement Depth (mbs) | Elevation of Well Site |
|---|---|---|---|---|---|---|---|
| **Massey #1** | 38.7675333 N, 108.81453 W | 320.3 m | 0 mbs | 92% | No | N/A | 1993 m |
| **Massey #2** | 38.767429 N, 108.814722 W | 343.2 m | 280 mbs | 25% | Yes | 328.6 m | 1993 |
| **UDR 1A** | 38.780381 N, 108.870376 W | 426 m | 200 mbs | 60% | Yes | Under study | 1924 m |
| **UDR 2A** | 38.782692 N, 108.851083 W | 359.6 m | 262 mbs | | Yes | 314 | 1974 |

**ESTIMATED* PALEO-RELIEF OF WELL SITE LOCATIONS**

| | North Rim** | South Rim*** |
|---|---|---|
| **Massey #1** | 887 m | 1131 m |
| **Massey #2** | 895 m | 1140 m |
| **UDR 1A** | 1000 m | 1250 m |
| **UDR 2A** | 902 m | 1146 m |

**Based on lowest known base elevation of approximate basement contact and modern elevation at each well site location*

***2560 m Elevation*

****2804 m Elevation*

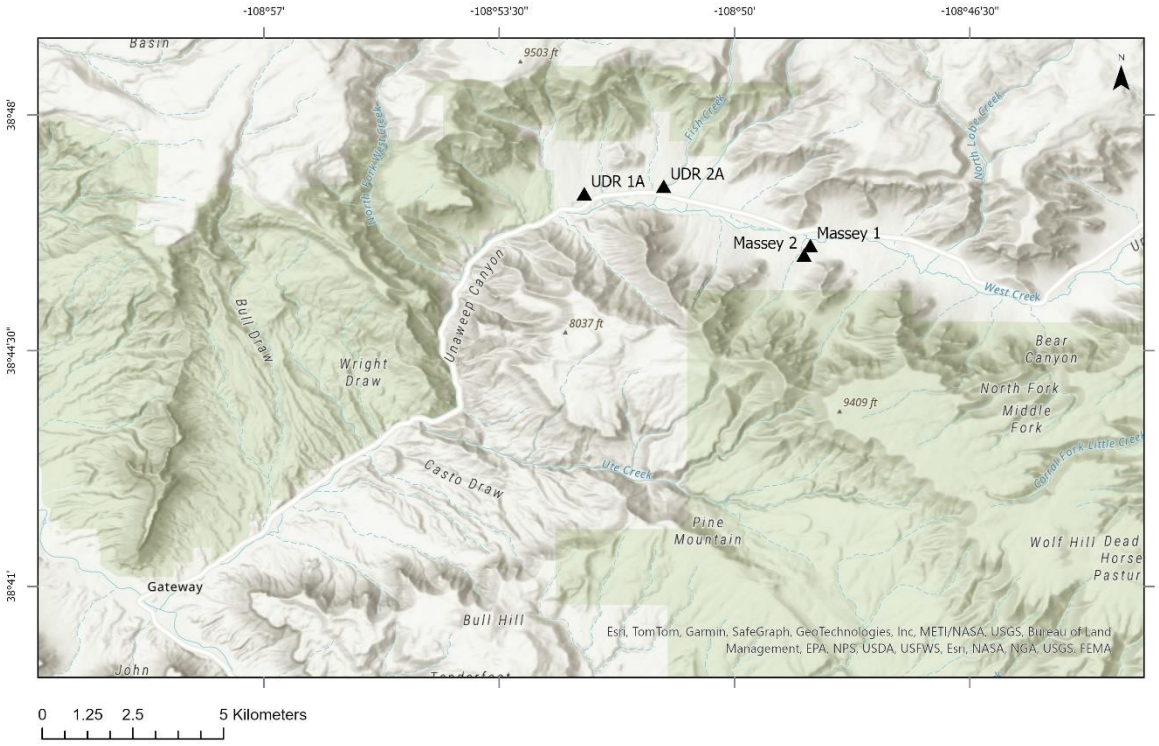



*Figure 1: Locations of Unaweep Canyon drilling well sites (Massey #1 and #2, UDR 1A, UDR 2A).*

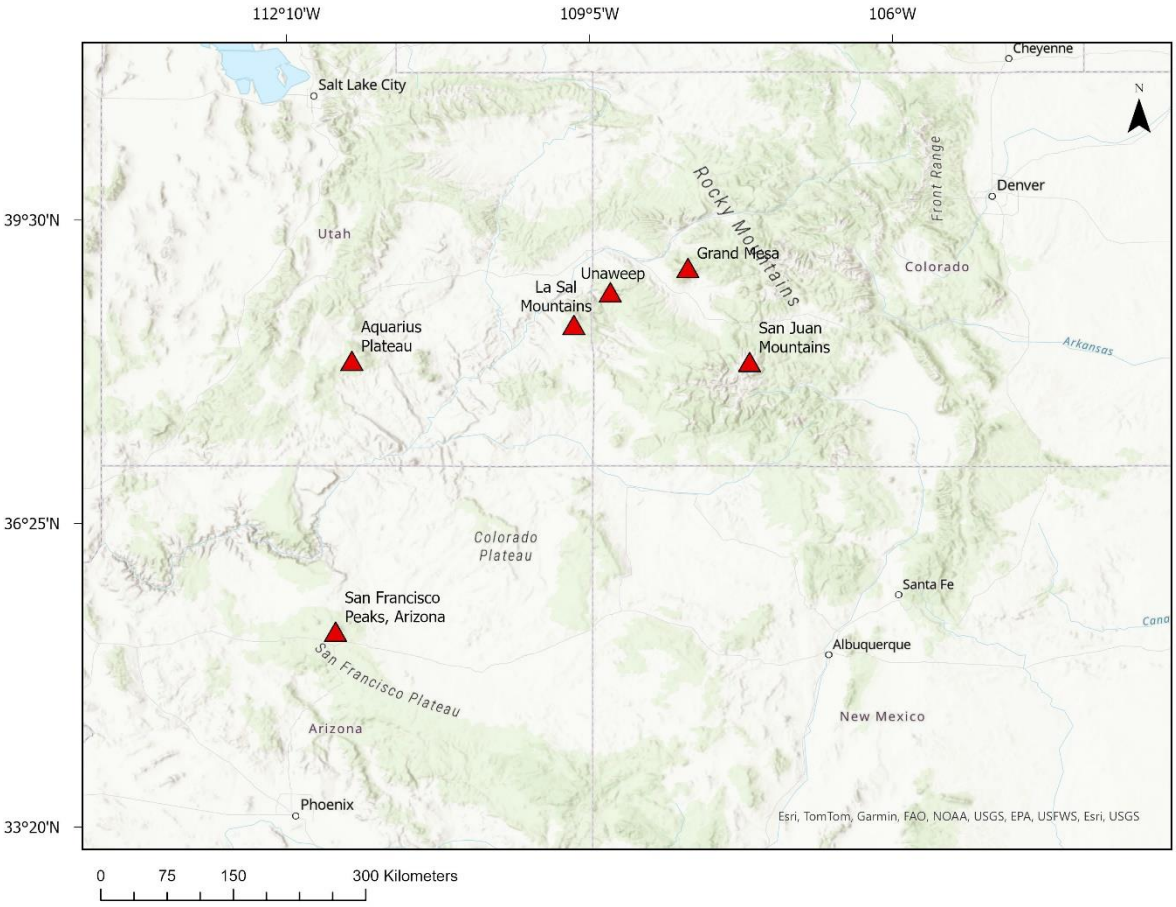



*Figure 2: Locations with recent alpine glaciation in regions surrounding the study area.*

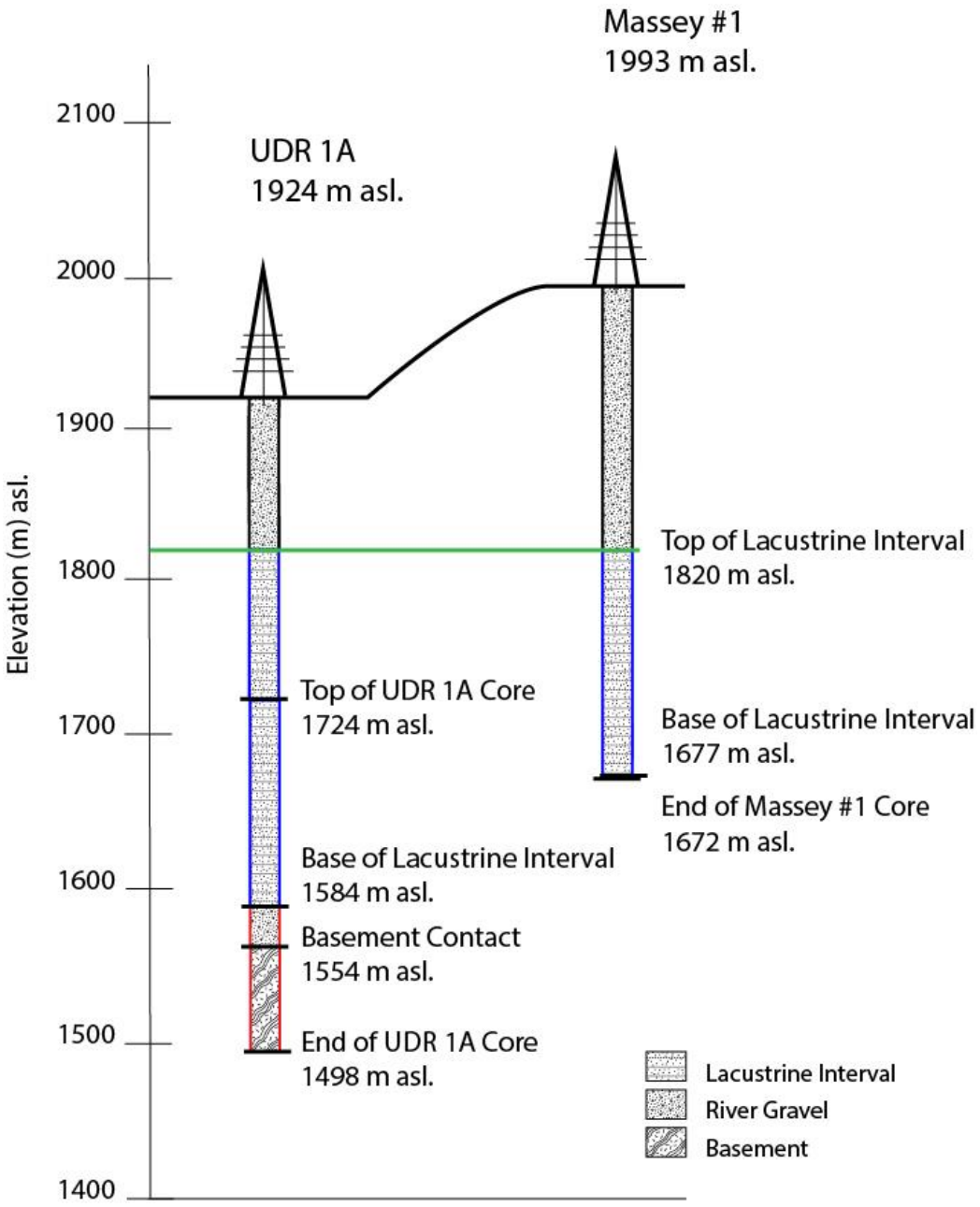



*Figure 3: Massey #1 and UDR 1A Core Depths*

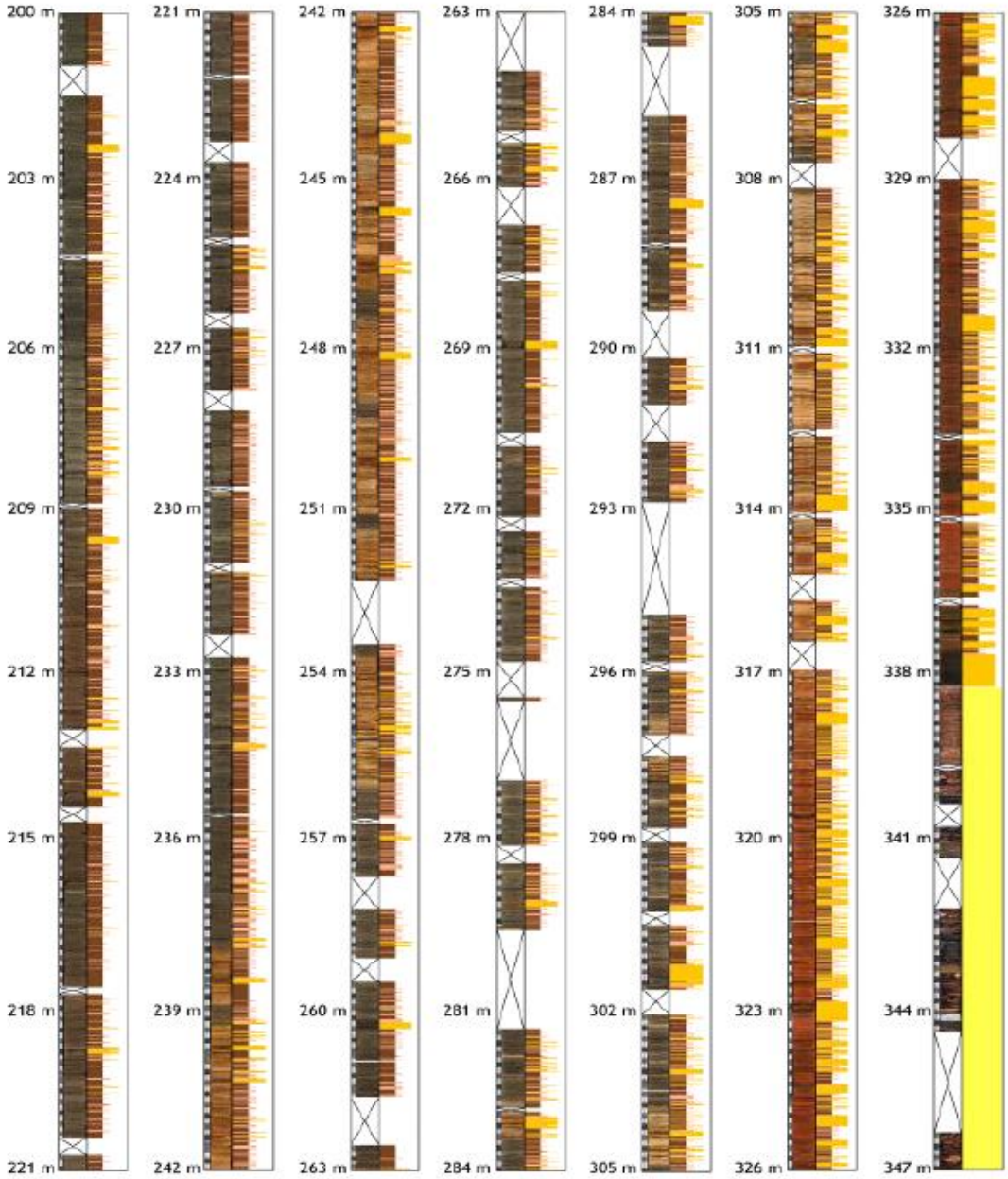



*Figure 4: UDR 1A condensed core sedimentology from Harris (2023).*

-Clay/Silt
-Very Fine Sand/Medium Sand
-Coarse Sand/Very Fine Gravel
-Gunnison Gravels

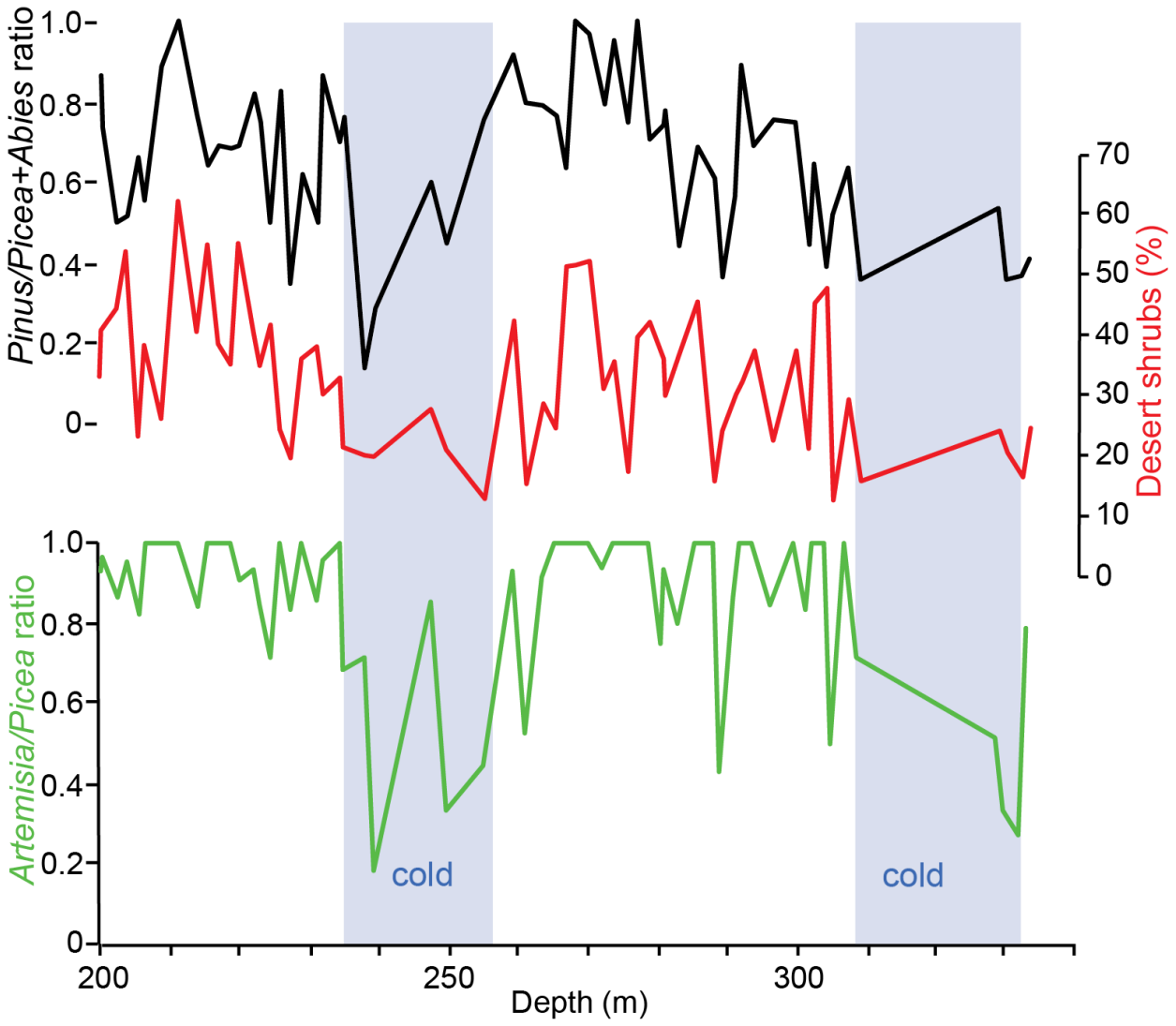



*Figure 5: Preliminary palynology assemblages analysis used for paleoclimate inferences. Artemisia/Picea ratio and P. edulis percentages showcasing two cold and two warm cycles (From G. Jimenez-Moreno).*

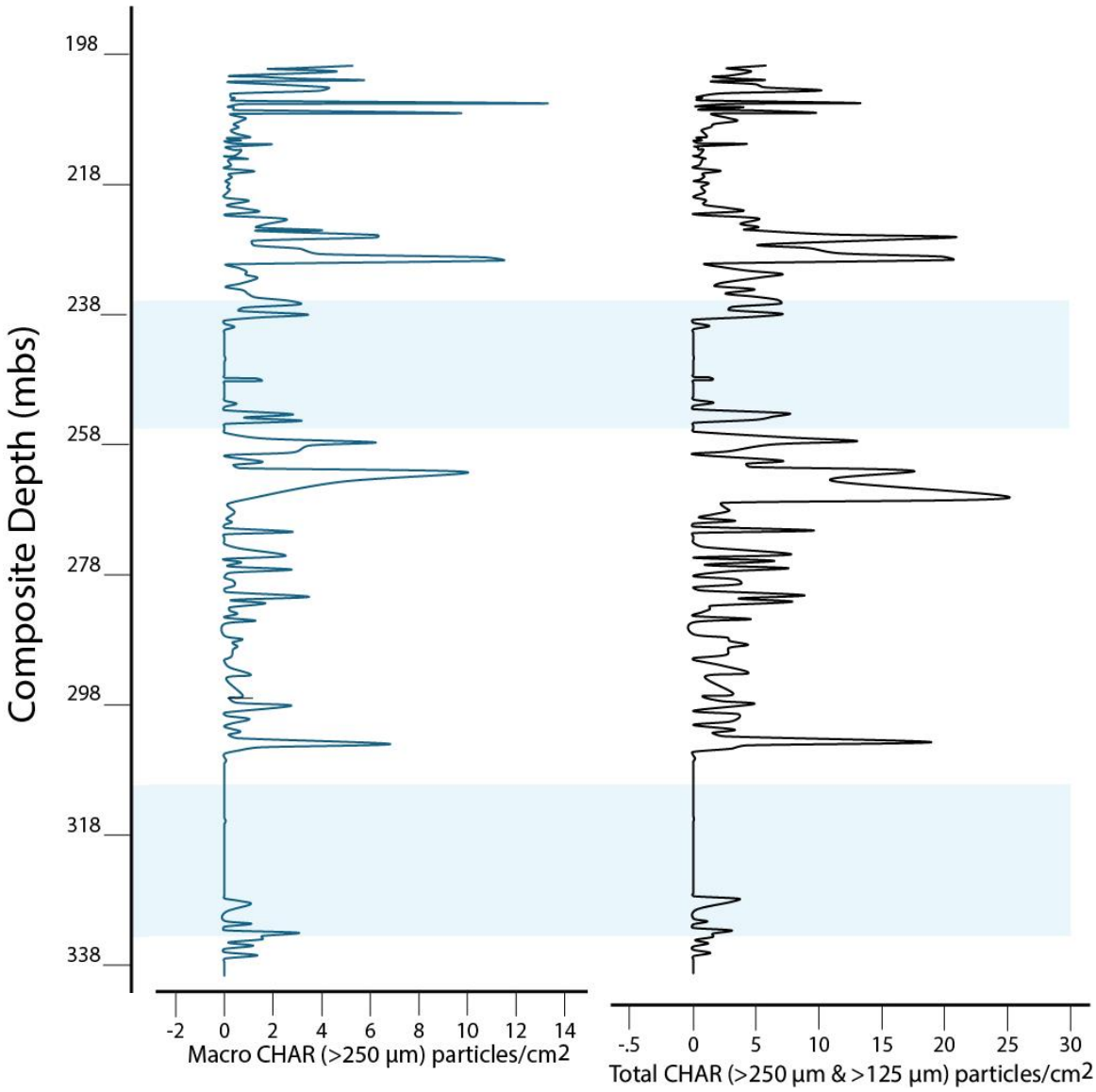



*Figure 6: Macro charcoal concentrations and total charcoal concentrations (particles/cm2) (right plot) throughout the UDR 1A core.*

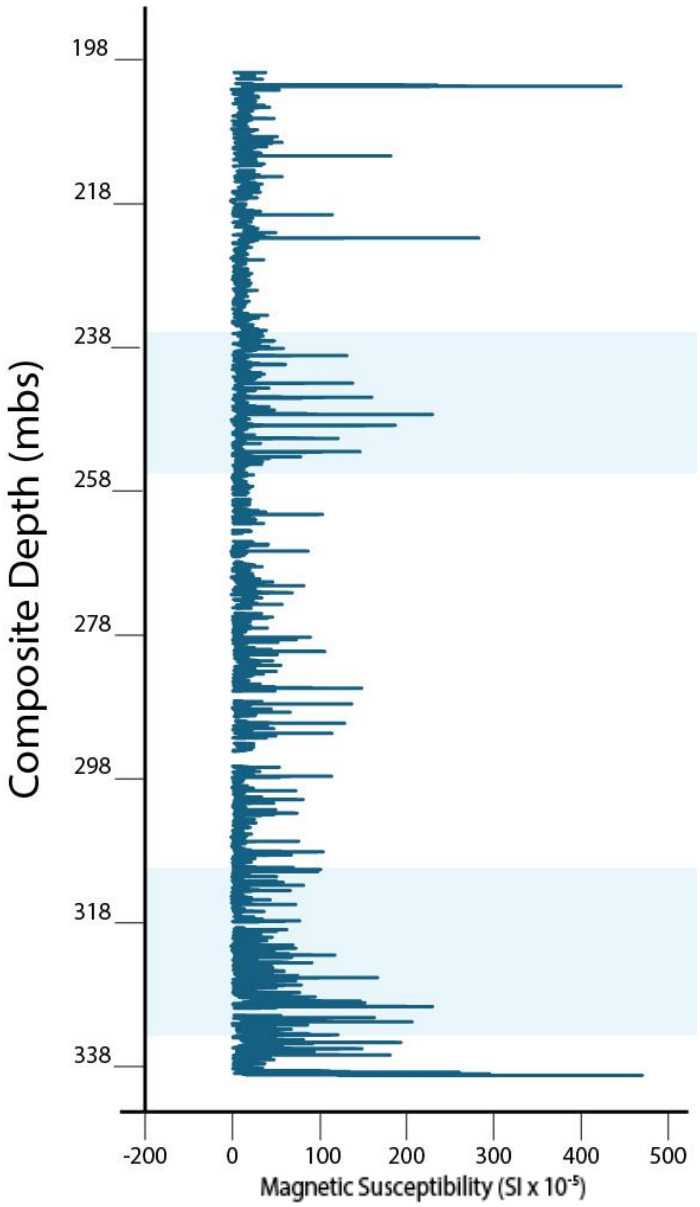



*Figure 7: Magnetic Susceptibility throughout the UDR 1A core. Depths 339.26 – 340.04 mbs are not displayed in this figure due to high MS values and scale proportions of lower values.*

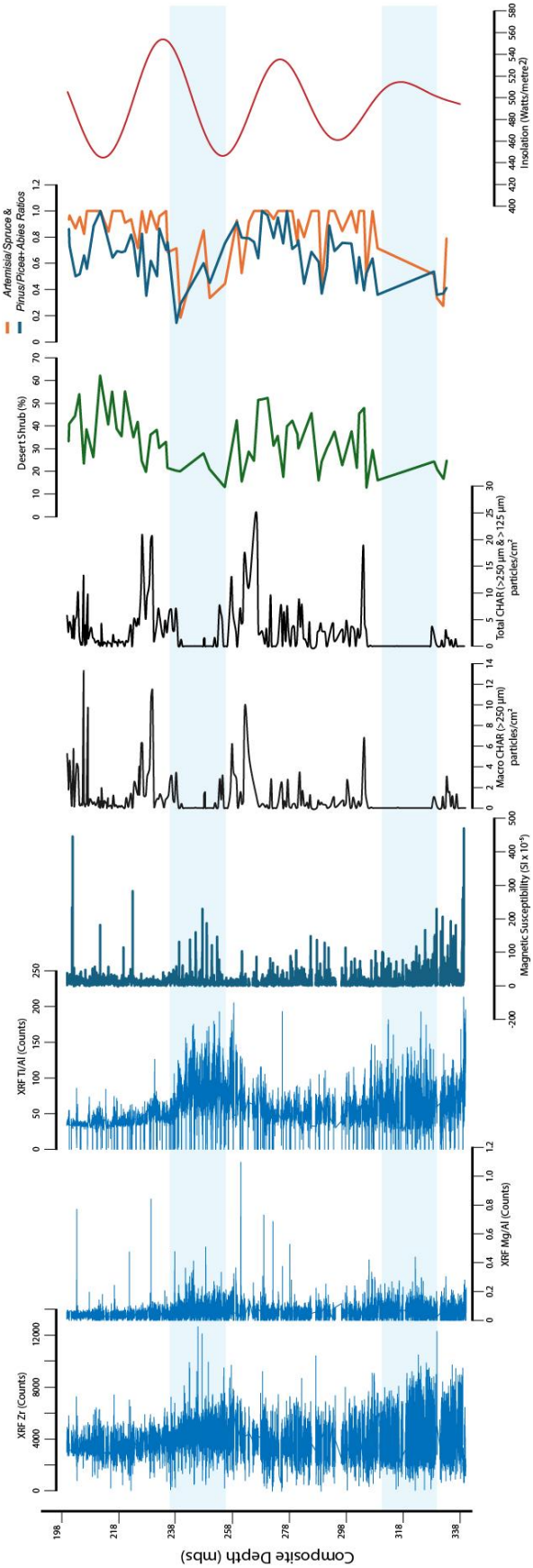



*Figure 8: Paleoclimate and paleofire indicators of core UDR 1A. From bottom to top: XRF Zr (counts), XRF Mg/Al (counts), XRF Ti/Al (counts), Magnetic Susceptibility SI x $10^{-5}$, Macro CHAR (>250 µm) particles/$cm^2$, Total CHAR (>250 µm & 125 µm) particles/$cm^2$, Desert Shrub (%), Artemisia/ Spruce and Pinus/Picea+Abies ratios, Insolation (watts/$metre^2$)*